

Manuscript Details

Manuscript number	ADWR_2017_99
Title	Application of a hybrid multiscale approach to simulate hydrologic and biogeochemical processes in the river-groundwater interaction zone
Article type	Research Paper

Abstract

The groundwater-surface water interaction zone (GSIZ) plays an important role in riverine and watershed ecosystems as the exchange of waters of variable composition and temperature (hydrologic exchange flows) stimulate microbial activity and associated biogeochemical reactions. Variable temporal and spatial scales of hydrologic exchange flows, heterogeneity of the subsurface environment, and complexity of biogeochemical reaction networks in the GSIZ present challenges to incorporation of fundamental process representations and model parameterization across a range of spatial scales (e.g. from pore-scale to field scale). This paper presents a novel hybrid multiscale simulation approach that couples hydrologic-biogeochemical (HBGC) processes between two distinct length scales of interest. Our multiscale simulation approach is tested and demonstrated on a two-dimensional (2D) domain that intersects the aquifer and the adjacent Columbia River within the 300 Area of the U. S. Department of Energy's Hanford Site. This domain is characterized by temporally dynamic intrusion of river water, aquifer contaminant plumes that interact with hydrologic exchange flows, and complex biogeochemistry driven by mixed sources of organic carbon. Microbial activity and biogeochemical reactions are focused in a relatively thin zone (1-2 m thick) immediately underlying and adjacent to the river, comprising recent riverbed sediments and referred to here as the alluvium layer. Within this layer, it has been hypothesized that biogeochemical reactions are strongly impacted by flow variations associated with permeability heterogeneity, and therefore may require unusually high spatial resolution of processes and material properties within the alluvium (microscale domain), relative to the full model domain (macroscale domain). Use of a fine grid over the full macroscale domain would be computationally inefficient and perhaps infeasible for three-dimensional domains of larger size. Additionally, the biogeochemistry within the alluvium layer is more complex than that of the rest of the macroscale domain, warranting use of different BGC reaction networks in the two domains. One approach to address these challenges is the application of a hybrid multiscale method that loosely couples high-fidelity simulations in the microscale domain with low-fidelity simulations in the macroscale domain. In the hybrid multiscale modeling workflow demonstrated and tested here, simulations at both scales employ the PFLOTRAN code. However, at the microscale, a grid with finer resolution is employed together with a complex BGC reaction network, while at the macroscale a simplified reaction network is utilized with a coarsely-resolved model grid. A scripted workflow using the Swift computational workflow environment is used to execute, monitor and couple microscale and macroscale simulations. The coupling is loose and is accomplished through iterated input-output file transfers. The approach, previously demonstrated for coupling pore- and continuum-scale reactive transport simulations, is applied here to couple multiple scales of continuum models over a field-scale domain. We test the accuracy and efficiency of our hybrid multiscale simulation by comparison with equivalent single-scale models, and then apply the multiscale model to numerically investigate the potential impacts of small-scale heterogeneity and different BGC reaction models.

Keywords hybrid multiscale simulation; loose coupling; groundwater-surface water interaction; hydrologic-biogeochemical processes

Taxonomy Biogeochemistry, Multiscale Analysis, Subsurface Hydrology, Groundwater

Corresponding Author Xiaofan Yang

Corresponding Author's Institution Pacific Northwest National Laboratory

Order of Authors Xiaofan Yang, Xuehang Song, Hyun-Seob Song, Zhangshuan Hou, Xingyuan Chen, Glenn Hammond, Yuanyuan Liu, Timothy Scheibe

Suggested reviewers Albert Valocchi, Matthew Balhoff, Ciaran Harman, Diogo Bolster, Ilenia Battiatto

Submission Files Included in this PDF

File Name [File Type]

cover letter.doc [Cover Letter]

Multiscale_pnnl_AWR.docx [Manuscript File]

To view all the submission files, including those not included in the PDF, click on the manuscript title on your EVISE Homepage, then click 'Download zip file'.

Tel: (509) 375-6867
Fax: (509) 372-6089
MSIN: K9-33
xiaofan.yang@pnnl.gov

February 6th 2017

Dear Prof. D'Odorico, Prof. Sander:

Please find enclosed a manuscript entitled "Application of a hybrid multiscale approach to simulate hydrologic and biogeochemical processes in the river-groundwater interaction zone" by Xiaofan Yang et al., which we wish to submit for publication in *Advances in Water Resources*. The manuscript was prepared using Microsoft Word and creates a 36-page document in 1.5-spaced format.

This paper presents a novel hybrid multiscale simulation approach that couples hydrologic-biogeochemical (HBGC) processes between two distinct length scales of interest in the river-groundwater interaction zone. Our multiscale simulation approach is tested and demonstrated on a two-dimensional (2D) domain that intersects the aquifer and the adjacent Columbia River within the 300 Area of the U. S. Department of Energy's Hanford Site. This domain is characterized by temporally dynamic intrusion of river water, aquifer contaminant plumes that interact with hydrologic exchange flows, and complex biogeochemistry driven by mixed sources of organic carbon. Microbial activity and biogeochemical reactions are focused in a relatively thin zone (1-2 m thick) immediately underlying and adjacent to the river, comprising recent riverbed sediments and referred to here as the alluvium layer. Within this layer, it has been hypothesized that biogeochemical reactions are strongly impacted by flow variations associated with permeability heterogeneity, and therefore may require unusually high spatial resolution of processes and material properties within the alluvium (microscale domain), relative to the full model domain (macroscale domain). Use of a fine grid over the full macroscale domain would be computationally inefficient and perhaps infeasible for three-dimensional domains of larger size. Additionally, the biogeochemistry within the alluvium layer is more complex than that of the rest of the macroscale domain, warranting use of different BGC reaction networks in the two domains. The current multiscale approach loosely couples high-fidelity simulations in the microscale domain with low-fidelity simulations in the macroscale domain.

In the hybrid multiscale modeling workflow demonstrated and tested here, simulations at both scales employ the PFLOTRAN code. However, at the microscale, a grid with finer resolution is employed together with a complex BGC reaction network, while at the macroscale a simplified reaction network is utilized with a coarsely-resolved model grid.

A scripted workflow using the Swift computational workflow environment is used to execute, monitor and couple microscale and macroscale simulations. The coupling is loose and is accomplished through iterated input-output file transfers. The approach, previously demonstrated for coupling pore- and continuum-scale reactive transport simulations, is applied here to couple multiple scales of continuum models over a field-scale domain. We test the accuracy and efficiency of our hybrid multiscale simulation by comparison with equivalent single-scale models, and then apply the multiscale model to numerically investigate the potential impacts of small-scale heterogeneity and different BGC reaction models.

Regarding the choice of referees, we will leave to your better judgment the selection of individuals that you feel can best offer constructive feedback on our manuscript. Researchers that we feel are especially well-qualified include

Prof. Albert Valocchi (University of Illinois at Urbana-Champaign, valocchi@illinois.edu),
Prof. Matthew Balhoff (University of Texas at Austin, balhoff@mail.utexas.edu),
Prof. Ilenia Battiatto (Stanford University, ibattiat@stanford.edu)
Prof. Diogo Bolster (University of Notre Dame, bolster@nd.edu) and
Prof. Ciaran Harman (Johns Hopkins University, charman1@jhu.edu).

On behalf of my co-authors, I wish to thank you for your time and consideration of our manuscript. We look forward to hearing from you in due course.

Yours sincerely,



Xiaofan Yang
Hydrology Technical Group
Energy and Environment Directorate
Pacific Northwest National Laboratory



1
2
3
4 1
5 2
6 3
7 4
8 5
9 6
10 7 **Application of a hybrid multiscale approach to simulate hydrologic and**
11 8 **biogeochemical processes in the river-groundwater interaction zone**

12 Xiaofan Yang^{1*}, Xuehang Song¹, Hyun-Seob Song¹, Zhangshuan Hou¹, Xingyuan Chen¹, Glenn
13 E Hammond², Yuanyuan Liu¹, Timothy D Scheibe^{1*}

14 ¹ Pacific Northwest National Laboratory, P.O. Box 999, Richland, WA 99354, USA

15 ² Sandia National Laboratories, Albuquerque, NM, USA

29 *Corresponding author: xiaofan.yang@pnnl.gov ; tim.scheibe@pnnl.gov

30 Submitted to *Advances in Water Resources*

57
58
59
60 **31 Abstract**

61 The groundwater-surface water interaction zone (GSIZ) plays an important role in riverine and
62 watershed ecosystems as the exchange of waters of variable composition and temperature
63 (hydrologic exchange flows) stimulate microbial activity and associated biogeochemical
64 reactions. Variable temporal and spatial scales of hydrologic exchange flows, heterogeneity of
65 the subsurface environment, and complexity of biogeochemical reaction networks in the GSIZ
66 present challenges to incorporation of fundamental process representations and model
67 parameterization across a range of spatial scales (e.g. from pore-scale to field scale). This paper
68 presents a novel hybrid multiscale simulation approach that couples hydrologic-biogeochemical
69 (HBGC) processes between two distinct length scales of interest.
70
71

72 Our multiscale simulation approach is tested and demonstrated on a two-dimensional (2D)
73 domain that intersects the aquifer and the adjacent Columbia River within the 300 Area of the U.
74 S. Department of Energy's Hanford Site. This domain is characterized by temporally dynamic
75 intrusion of river water, aquifer contaminant plumes that interact with hydrologic exchange
76 flows, and complex biogeochemistry driven by mixed sources of organic carbon. Microbial
77 activity and biogeochemical reactions are focused in a relatively thin zone (1-2 m thick)
78 immediately underlying and adjacent to the river, comprising recent riverbed sediments and
79 referred to here as the alluvium layer. Within this layer, it has been hypothesized that
80 biogeochemical reactions are strongly impacted by flow variations associated with permeability
81 heterogeneity, and therefore may require unusually high spatial resolution of processes and
82 material properties within the alluvium (microscale domain), relative to the full model domain
83 (macroscale domain). Use of a fine grid over the full macroscale domain would be
84 computationally inefficient and perhaps infeasible for three-dimensional domains of larger size.
85 Additionally, the biogeochemistry within the alluvium layer is more complex than that of the rest
86 of the macroscale domain, warranting use of different BGC reaction networks in the two
87 domains. One approach to address these challenges is the application of a hybrid multiscale
88 method that loosely couples high-fidelity simulations in the microscale domain with low-fidelity
89 simulations in the macroscale domain.
90
91

92 In the hybrid multiscale modeling workflow demonstrated and tested here, simulations at both
93 scales employ the PFLOTRAN code. However, at the microscale, a grid with finer resolution is
94
95

113
114
115 61 employed together with a complex BGC reaction network, while at the macroscale a simplified
116 62 reaction network is utilized with a coarsely-resolved model grid. A scripted workflow using the
117 63 Swift computational workflow environment is used to execute, monitor and couple microscale
118 64 and macroscale simulations. The coupling is loose and is accomplished through iterated input-
119 65 output file transfers. The approach, previously demonstrated for coupling pore- and continuum-
120 66 scale reactive transport simulations, is applied here to couple multiple scales of continuum
121 67 models over a field-scale domain. We test the accuracy and efficiency of our hybrid multiscale
122 68 simulation by comparison with equivalent single-scale models, and then apply the multiscale
123 69 model to numerically investigate the potential impacts of small-scale heterogeneity and different
124 70 BGC reaction models.

131
132 71
133
134 72 Key words: hybrid multiscale simulation; loose coupling; groundwater-surface water interaction;
135 73 hydrologic-biogeochemical processes

137 74

139 75

141 76

143 77

145 78

147 79

149 80

151 81

153 82

155 83

157 84

159 85

160 86

162 87

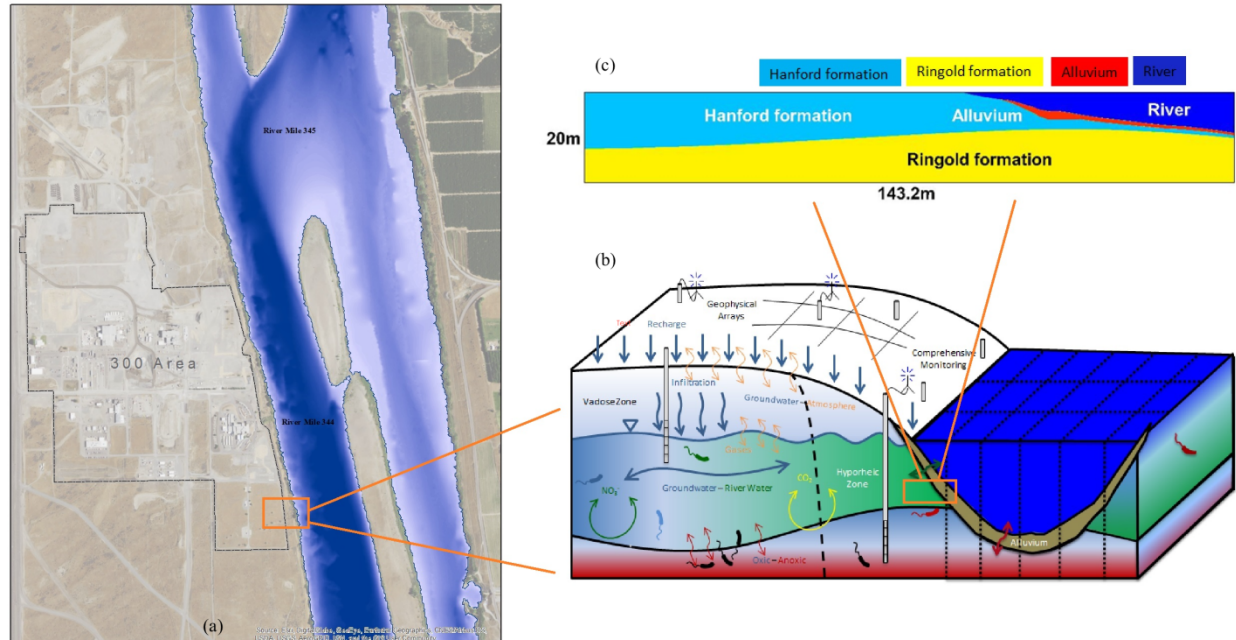
169
170
171 88 **1. Introduction**
172
173

174 89 The groundwater-surface water interaction zone (GSIZ), the region of the subsurface below or
175 90 adjacent to a river or stream into which surface water exchanges occur, has been recognized as
176 91 an ecologically and biogeochemically active zone that plays a critical role in river ecosystems
177 92 [Findlay, 1996; Brunke and Gonser, 1997; Smith, 2005; Larned et al., 2015]. It is also a key
178 93 element of the earth critical zone (land surface-soil-water-atmosphere interaction zone)
179 94 [<http://criticalzone.org/national/>]. Movement of surface water into and out of the GSIZ (referred
180 95 to as hydrologic exchange flows [Harvey and Gooseff, 2015]) leads to mixing of waters
181 96 containing variable levels of dissolved oxygen (DO), dissolved organic carbon (DOC), nutrients,
182 97 contaminants, and other solutes, and thereby gives rise to complex coupled hydrologic-
183 98 biogeochemical (HBGC) processes [Boano, 2014; Cardenas, 2015]. Among those processes,
184 99 microbially-mediated aerobic respiration of organic carbon, nitrification and denitrification are
185 100 considered to be important [Findlay, 1995; Bencala, 2000; Pinay et al., 2015], and can be related
186 101 to other redox-sensitive reactions. Field experiments [Packman et al., 2004; Kessler et al., 2012;
187 102 Fox et al., 2014], column experiments with hyporheic zone sediments [Doussan et al., 1997; Gu
188 103 et al., 2007; Yan et al., 2016; Liu et al., 2017] and numerical modeling studies [Mayer et al.,
189 104 2002; Storey et al., 2003; Lautz and Siegel, 2006; Fleckenstein et al., 2010; Brunner et al., 2010;
190 105 Frei et al., 2012; Gu et al., 2012; Janssen et al., 2012; Han et al., 2014; Krause et al., 2014; Chen
191 106 et al., 2015; Liggett et al., 2015] have all been useful in improving our understanding of solute
192 107 transport and biogeochemical turnover processes in the GSIZ. A number of studies have
193 108 successfully used numerical models to simulate results of field studies and laboratory
194 109 experiments [Boano et al., 2009; Fleckenstein et al., 2010; Frei et al., 2012; Gu et al., 2012;
195 110 Janssen et al., 2012; Han et al., 2014; Krause et al., 2014; Trauth et al., 2013; Trauth et al., 2014],
196 111 by providing detailed understanding of the controlling mechanisms and dynamic distributions of
197 112 the processes within the GSIZ. However, three major issues pose challenges to field-scale
198 113 numerical modeling of HBGC processes in the GSIZ. Firstly, hydrogeological structures in the
199 114 GSIZ are often complex and exhibit strong physical and biogeochemical heterogeneity that can
200 115 greatly impact HBGC processes. Secondly, river discharge (and therefore river stage) can vary
201 116 over a range of temporal scales from hourly to multi-year, leading to dynamic hydrologic
202 117 exchange flows and complexities in microbiological responses that introduce computational
203 118 challenges. Finally, because of multiple scales of physical and biogeochemical heterogeneity in
204
205
206
207
208
209
210
211
212
213
214
215
216
217
218
219
220
221
222
223
224

225
226
227 natural systems, HBGC processes in the GSIZ often require scale-dependent parameterizations
228 and/or process representations, and the interactions among processes at different scales are
229 poorly understood and difficult to predict.
230
231
232 In summary, coupled HBGC processes in the GSIZ exhibit multi-scale and multi-physical
233 features (different mathematical representations of physical, biological and chemical processes at
234 distinct scales) that motivate the development of multiscale modeling approaches. Single-scale
235 simulations at low fidelity are computationally efficient, but require high levels of
236 parameterization that may inadequately represent impacts of microscopic physical/chemical
237 processes and their linkages to macroscopic phenomena [Wood, 2009; Gray et al., 2013]. Single-
238 scale simulations at high fidelity may offer higher predictive potential, but at high computational
239 expense [Molins, 2015; Yang et al., 2016]. In recent years, hybrid multiscale methods [E et al.,
240 2003; Ingram et al., 2004; Mehmani and Balhoff, 2015] have begun to be applied to study of
241 flow and transport processes in subsurface systems with multiscale heterogeneity. Scheibe et al.
242 [2015a] provide a review of several classes of multiscale methods including hybrid multiscale
243 methods, with discussion of recent applications to subsurface flow and reactive transport
244 simulation. Conceptually, hybrid multiscale methods describe the flow and reactive transport
245 processes using different mathematical models and parameters at each scale, and define coupling
246 schemes between models at different scales (e.g., Tartakovsky and Scheibe, 2011) to ensure
247 process continuity and exchange model parameters (e.g. reaction rate), states, and boundary
248 conditions. It is obvious that the coupling scheme between scales is the core and major challenge
249 of this method. Key factors to be considered include the consistency between models, data
250 exchange and I/O control, and computational efficiency. A variety of different hybrid methods
251 have been developed and applied, such as the hybrid mortar method [Balhoff et al., 2008;
252 Mehmani and Balhoff, 2014; Tang et al., 2015], iterative boundary coupling [Battiato et al.,
253 2011], non-iterative coupling of Smoothed Particle Hydrodynamics (SPH, Tartakovsky et al.,
254 2010), and the hybrid multiscale finite volume (h-MsFV) method [Tomin and Lunati, 2013;
255 Tomin and Lunati, 2015; Barajas-Solano and Tartakovsky, 2016]. A hybrid loose coupling
256 method based on the heterogeneous multiscale method of E et al. [2003] was developed by our
257 team and previously applied to coupled pore- and Darcy-scale simulation of reactive transport
258 [Scheibe et al., 2015b, 2015c]. The loose coupling method employs user-specification of input
259 and output files passed to and from each at-scale simulator, together with functional descriptions
260
261
262
263
264
265
266
267
268
269
270
271
272
273
274
275
276
277
278
279
280

281
282
283 150 (subdomain determination and upscaling/downscaling schemes) used for data exchange between
284 151 scales, in a Swift-controlled high-performance computing workflow environment [Wilde et al.,
285 152 2011]. The script-based multiscale modeling framework was tested using a mixing-controlled
286 153 reaction in a homogeneous porous media system [Scheibe et al., 2015b], in which microscale
287 154 (pore-scale) and macroscale (continuum-scale) reactive transport models were loosely coupled.
288 155 Most of the previous hydrogeologic applications of hybrid multiscale methods have been used to
289 156 couple flow and reactive transport from pore scale to continuum scale in synthetic porous media,
290 157 with limited focus on field-scale applications. In the current study, we apply the same loose-
291 158 coupling modeling framework to simulate field-scale groundwater-river water mixing and its
292 159 impacts on HBGC processes (carbon and nitrogen biogeochemistry) in the GSIZ.
293
294
295
296
297
298 160 The current study is based on a field research site at the 300 Area of the U. S. Department of
301 161 Energy's (DOE) Hanford Site [Zachara et al., 2013]. The site is located in a semi-arid region and
302 162 is bordered by the Columbia River (Figure 1a). Interest in field-scale models applied over
303 163 domains hundreds of meters in size is motivated by the existence of contaminant plumes near the
304 164 river [Hammond and Lichtner, 2010]. The plumes are impacted by river water intrusion that can
305 165 extend significant distances inland [Johnson et al., 2015], and by biogeochemical processes that
306 166 are relatively high in the GSIZ [Moser et al., 2003]. Modeling coupled hydrologic and
307 167 biogeochemical processes in this context is challenging because 1) biogeochemical activity is
308 168 enhanced in a relatively thin zone of recent river alluvium (1-2 meters thick) immediately
309 169 underlying the river (referred to as the alluvial layer, Figure 1b) relative to the surrounding
310 170 aquifer materials; 2) hydrobiogeochemical processes may be strongly impacted by small-scale
311 171 physical and biogeochemical heterogeneity within the alluvial layer; and 3) the biogeochemical
312 172 reactions in the alluvial layer are more complex than those in the surrounding aquifer. Therefore,
313 173 a more sophisticated level of simulation may be required for accuracy in the thin alluvial layer
314 174 (higher resolution and complex biogeochemical reaction network) while maintaining a simpler
315 175 model in the rest of the model domain for computational efficiency. Hybrid multiscale
316 176 simulation offers a potential approach to meet these competing objectives. The loose coupling
317 177 approach used in our previous studies was adapted to this problem. In this application both
318 178 model scales (the alluvial layer – microscale domain -- and the rest of the system – macroscale
319 179 domain, Figure 1c) are simulated using the open-source PFLOTRAN flow and reactive transport
320 180 simulation code [Lichtner et al., 2013]. However, at the microscale a computational grid with
321
322
323
324
325
326
327
328
329
330
331
332
333
334
335
336

337
 338
 339
 181 finer resolution is employed together with a more complex biogeochemical reaction network,
 340 while at the macroscale a simplified reaction network is utilized with a coarsely-resolved model
 341 grid. Table 1 summarizes the attributes of the microscale and macroscale models. Customized
 342 scripts were developed for coupling schemes and exchange of data between scales. The entire
 343 multiscale simulation framework is executed in the Swift-based environment on high
 344 performance computing clusters.
 345
 186
 347
 348
 349



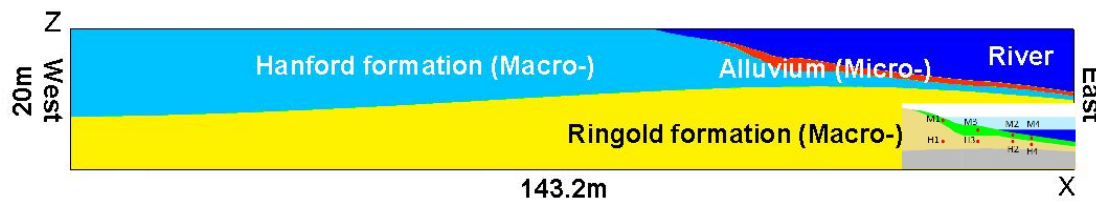
189 Figure 1. Schematic diagrams of the modeling domain: (a) Hanford 300A study site;
 371 (b) the GSIZ; (c) the
 190 current 2D modeling domain.

191
 374 Table 1. Multiscale modeling framework for flow and reactive transport
 375

Scale\Model	Facies	Formation	Flow model	BGC model	Grid	Solver
Macro-scale	Subsurface	Hanford+Ringold	Richards Equation	Gu et al. 2012	Coarse	PFLOTRAN
Micro-scale	Riverine	Alluvium	Richards Equation	Song et al. 2017	Fine	PFLOTRAN

393
394
395
396 195 The rest of the paper is organized as follows: Section 2 introduces the modeling domain and
397 setup (including hydrogeological properties assigned in the domain and the biogeochemical
398 reaction network models); Section 3 explains the hybrid multiscale simulation framework and its
399 execution; Section 4 presents results and discussion followed by concluding remarks.
400
401
402 199
403
404 200 **2. Hanford 300A Site Model Configuration**
405
406 201 The hybrid multiscale modeling framework simulates subsurface flow and reactive transport.
407
408 202 Subsurface flow is simulated on a 2D cross-sectional domain (Figure 2), with dynamic head
409 boundary conditions specified from observations of river water stage (river boundary) and
410 interpolation of observations from inland wells (aquifer boundary). Reactive transport
411 simulations are based on a combination of previously published (Gu et al., 2012) and newly
412 developed (Song H.-S., et al., 2017) biogeochemical network models describing aerobic
413 respiration and denitrification. The 2D computational domain is that same as that used by our
414 team to investigate the impact of dam operation and hydropeaking on HBGC processes (Song X.
415 et al., 2017). We use this 2D domain here for simplicity, and to facilitate comparisons with
416 independent simulation outputs (such as a single-scale simulation with uniformly fine grid
417 resolution). We recognize that this 2D system could be represented at high resolution over the
418 entire domain without undue computational demand, and therefore does not require the hybrid
419 multiscale approach. However, this test system allows us to develop, test and demonstrate our
420 approach prior to application to larger 3D domains for which the computational efficiency of the
421 hybrid method would be more advantageous.
422
423
424
425
426
427
428
429
430
431 216 *2.1. Computational domain and setup*
432
433 217 The 2D model domain is shown in Figure 2. The dimensions of the domain are 143.2 m by 20 m,
434 with the elevation ranging from 90 m to 110 m. A sloping bank represents the geometry of the
435 groundwater-river water interface. The modeling domain comprises three stratigraphic
436 formations with different hydrogeological properties [Williams et al., 2000; Williams et al.,
437 2008; Zachara et al., 2012]: alluvium layer (recent fluvial deposits with low permeability),
438 Hanford formation (gravels with high permeability) and Ringold formation (ancient semi-
439 consolidated fluvial deposits with low permeability). The boundaries and shapes of the
440 formations are based on previous field surveys and measurements at the extensively-studied
441
442
443
444
445
446
447
448

449
 450
 451 225 300A site. As mentioned above, the alluvium is a thin layer (1-2 m thick) adjacent to the river,
 452 but with disproportionate impact on flow and biogeochemical reactions. Both homogeneous and
 453 heterogeneous property distributions are considered for the aquifer properties in the current
 454 study. For homogeneous scenarios, hydraulic conductivity is assumed to be constant within each
 455 formation with values as listed in Table 2. For heterogeneous scenarios, the spatial distributions
 456 of the hydraulic conductivities in the modeling domain were defined using geostatistical models
 457 explained in Section 2.3. Four sets of hypothetical well observation points (marked by red dots in
 458 Figure 2) are located in the alluvium layer and the Hanford formation.
 459
 460
 461
 462
 463



483
 484
 485
 486
 487
 488

Parameters\Formations	Hanford	Ringold	Alluvium
Porosity	0.2	0.43	0.43
Permeability	7.387e-9	1.055e-12	3.864e-11

489 242
 490
 491 243 *2.2. Geostatistical model of physical heterogeneity*
 492
 493 244 Hydrogeological properties vary naturally through space as a result of the complex geologic
 494 processes through which aquifers evolve. The heterogeneity of hydraulic conductivity (K) exerts
 495 control on the movement of water and solutes in groundwater and through surface water-
 496 groundwater interfaces. Hydraulic conductivity can vary by several orders of magnitude over
 497 short distances. However, there is rarely sufficient data to deterministically prescribe these
 498
 499
 500

505
506
507
508
509
510
511
512
513
514
515
516
517
518
519
520
521
522
523
524
525
526
527
528
529
530
531
532
533
534
535
536
537
538
539
540
541
542
543
544
545
546
547
548
549
550
551
552
553
554
555
556
557
558
559
560

249 heterogeneous spatial distributions. Accordingly, it has become common practice to use
250 stochastic approaches to incorporate spatial heterogeneity in hydraulic properties into numerical
251 models of subsurface fluid flow and transport [e.g., Gelhar, 1986; Wagner and Gorelick, 1989;
252 Rubin, 2003]. Various geostatistical simulation approaches can be used to generate multiple
253 realizations of heterogeneous fields of hydraulic conductivity, which are treated in this context as
254 spatial random functions. Gaussian geostatistical simulation is commonly used for continuous
255 data; it assumes that the data, or a transformation of the data, is multivariate Gaussian and
256 stationary (i.e., the mean, variance, and spatial structure (semivariogram) is constant in the
257 spatial domain) [Rubin and Journel, 1991; Deutsch and Journel, 1998].

258 The Hanford, Ringold, and recent alluvium geological units are each associated with different
259 erosional and depositional processes and therefore exhibit different characteristics of
260 heterogeneity [Hou et al., 2017]. The statistical moments of hydraulic conductivity (K) for the
261 Hanford and Ringold formations are inferred based on previous reports focused on the Columbia
262 River and Hanford Reach [Newcomb and Brown, 1961; Newcomb et al., 1972; Cass et al., 1981;
263 Williams et al., 2000; Vermeul et al., 2003, 2009; Last et al., 2006; Thorne et al., 2006; Fritz and
264 Arntzen, 2007; Fritz et al., 2007; Peterson et al., 2008; Williams et al., 2008; Truex et al., 2009;
265 Bjornstad et al., 2010; USDOE, 2010; Zachara et al., 2012], and the spatial semivariogram model
266 parameters are trained based on hydraulic conductivity measurements from an array of boreholes
267 in Hanford 300A (an exponential semivariogram model is used here). The anisotropy angles are
268 determined by assuming the maximum correlation direction is parallel to the interfaces between
269 the formations. Insufficient data are available for the alluvium layer to determine the correlation
270 length parameter, which is assumed here to be no more than 1 m since the parameter is scale-
271 dependent [Goovaerts and Webster, 1994; Davis et al., 1997; Di Fedrico and Neuman, 1997;
272 Dobermann et al., 1997] and the thickness of the alluvial layer is typically 1-2 meters. Table 3
273 summarizes the geostatistical parameters that are used for the simulations of $\log_{10}(K(m/d))$.

561
562
563
281
564
565

282 Table 3. Geostatistical parameters for three geostratigraphic formations in the modeling domain.

Parameters\Formations	Hanford	Ringold	Recent alluvium
Mean, $\log_{10}(m/d)$	3.077	0.8787	1.978
Variance/Sill	0.71	0.41	0.55
Max correlation range (m)	9.4	9.4	1.0
Anisotropy ratio	0.1	0.1	0.1
Nugget	0	0	0
Anisotropy angle (radians)	-0.052	-0.052	0.157

571
572
573
574
575
576
577
578
579
580
283
582
583
284
584
285
586
286
587
287
588
288
589
289
590
290
591
291
592
292
593
598
599
600
601
602
603
604
605
606
607
608
609
610
611
612
613
614
615
616

Figure 3 shows two representative realizations (for the alluvium and the entire domain, respectively) of the heterogeneous 2D field of $\log_{10}(K)$ generated based on the above parameters using the R geostatistical package geoR. To systematically evaluate the performance of the numerical model and understand how spatial heterogeneity (K) may affect the flow and transport processes in the study domain, multiple realizations are generated reflecting uncertainty in the specific configuration of the K field while honoring the global distribution and spatial correlation structure of the data. A small number of selected realizations are employed and tested in the current multiscale modeling study. Further studies using additional realizations and sensitivity analysis of parameters are continuing and will be reported in future manuscripts.

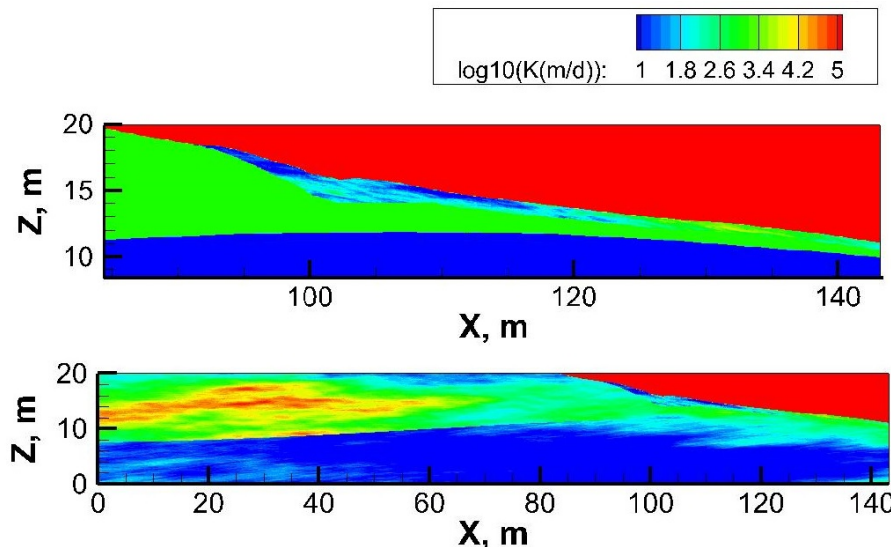


Figure 3. Two example realizations of the 2-D heterogeneity field of \log_{10} hydraulic conductivity (m/d).

2.3. Subsurface flow model

In PFLOTRAN, the groundwater model simulates variably saturated flows by solving the Richards equation described as follows:

$$\frac{\partial \varphi s \rho}{\partial t} + \nabla \cdot \mathbf{q} \rho = Q \quad (3.1)$$

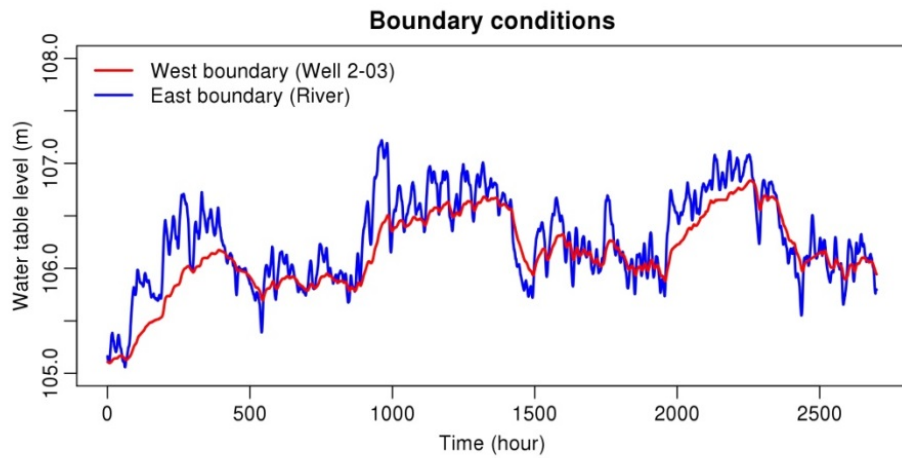
where φ denotes the porosity for each stratigraphic formation, s is the saturation, ρ is the fluid density, t is the time, \mathbf{q} is the Darcy velocity and Q is the source/sink term. For variably saturated flow, the unsaturated soil hydraulic conductivities (Section 2.2) are accounted for using the van Genuchten soil water retention model [van Genuchten, 1980]. The residual and saturated moisture contents and the associated parameters are determined from in situ soil characteristics.

Hydrostatic heads are applied to the entire modeling domain as initial conditions. Transient hydrostatic (variable head) boundary conditions are interpolated from observations and assigned to the inland (West) and river (East) boundaries (Figure 4) over a period of 2500 hr (short-term) for the current modeling application. Longer-term simulations with different objectives are described in Song X. et al. [2017]. The river stage varies 2 m or less over the short-term study period. The top and bottom boundaries of the domain are treated as no flow boundaries.

Recharge is not considered in the model.

673
674
675
676
677
678
679
680
681
682
683
684
685
686
687
688
689
690
691
692
693
694
695
696
697
698
699
700
701
702
703
704
705
706
707
708
709
710
711
712
713
714
715
716
717
718
719
720
721
722
723
724
725
726
727
728

313



314

315 Figure 4. Boundary conditions: seasonal river stage calibrated from field measurement and monitored
316 data from wells.

317

318 A standard finite volume method is used for discretization in PFLOTRAN (see user manual for
319 details). The grid resolution of the domain is initially uniform (0.1 m x 0.05 m) then nested (finer
320 resolution in alluvium) for multiscale simulations, which will be further explained in Section 3.
321 A time step of 1 hr was selected to ensure numerical stability. All numerical simulations were
322 conducted using National Energy Research Scientific Computing Center (NERSC)
323 supercomputers (Edison and Cori).

324

325 *2.4. Reactive transport and biogeochemical models*

326 Solute transport in PFLOTRAN is represented by the advective-dispersive equation based on the
327 simulated transient flow field:

$$328 \frac{\partial \varphi C_i}{\partial t} + \nabla \cdot (\mathbf{q}_i C_i - \varphi s \tau D \nabla C_i) = Q_{ci} \quad (3.2)$$

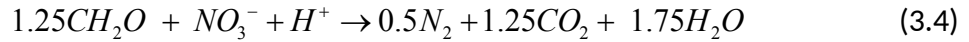
329 where C_i is the concentration of each species, D is the dispersion coefficient and Q_{ci} is the
330 source/sink term. The dispersion coefficients are constant in all directions with an assumed value
331 of $1e-9$ m 2 /s. The boundary conditions for the transport (inland and river) are based on averaged
332 sampling data from field measurements [Stegen et al., 2016].

729
730
731 333 As introduced in Section 1, two different biogeochemical (BGC) models were employed
732 334 concurrently: one for the alluvial layer [Song H.-S. et al., 2017] and second simpler model for
733 335 the rest of the domain [Gu et al., 2012]. Both BGC models represent aerobic respiration and
734 336 denitrification but utilize different reaction networks and reaction rates/coefficients.
735
736

737 337 Gu et al. [2012] developed a general Monod-type model to describe aerobic respiration
738
739



740 338 and denitrification
741
742



743 340 The reactants and products being monitored in the simulations include H^+ , CO_2 , CH_2O , O_2 , NO_3^-
744 341 and N_2 . The source term for the reactive transport of the species is calculated as:
745
746

$$Q_{ci} = R_i \mathbf{q}_i \quad (3.5)$$

747 343 where the reaction rates R_i are calculated using multiple Monod kinetics. The above model was
748 344 previously used to study flow and reactive transport under hyporheic exchanges in the riparian
749 345 zone, and has been tested and proved to be informative. Therefore we have adopted this model
750 346 for use in the Hanford and Ringold formations, with the associated parameters as described in Gu
751 347 et al. [2012].
752
753

754 349 The model of Song H.-S. et al. [2017] is based on laboratory experiments using 300A alluvium
755 350 sediments, and thus more specifically represents the microscale domain in the current study. This
756 351 new model places a focus on the description of microbial regulation as a key component of
757 352 biogeochemical modeling. Microbes regulate metabolism by controlling enzyme levels and
758 353 activities so that, when alternative electron donors and acceptors are available in environment,
759 354 they often preferentially use one over another instead of using them all simultaneously. Detailed
760 355 regulatory modeling will require information on molecular details, which are largely unknown,
761 356 however, except for specific processes. Consequently, in most of the biogeochemical modeling
762 357 studies, microbial regulation has been accounted for using empirical inhibition kinetics (e.g.,
763 358 Trauth et al., 2014; Gu et al., 2007). The cybernetic modeling approach developed Ramkrishna
764 359 and coworkers provides an alternative way to account for microbial regulation [Ramkrishna and
765 360 Song, 2012]. The cybernetic approach views organisms as teleonomic systems that regulate
766 361 metabolism to promote a certain metabolic objective in a varying environment. This postulate
767 362 leads to analytic forms of regulation rules (called the cybernetic control laws), which can be
768
769

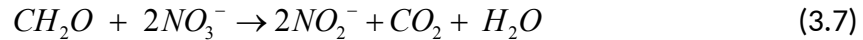
785
 786
 787 363 derived from an optimal control theory [Young and Ramkrishna, 2007]. In a previous study,
 788 364 Song and Liu [2015] demonstrated how the cybernetic modeling could be successfully applied to
 789 365 model denitrifying organisms. In the extension to microbial communities, Song H.-S. et al.
 790 366 [2017] provided two versions of the cybernetic model: genetically structured and simplified
 791 367 models. Below, we provide a summary of the simplified cybernetic model.
 792
 793

794 368 Based on data from the laboratory column experiments [Li et al., 2016], the microbially
 795 369 mediated biogeochemical processes are modeled by accounting for aerobic respiration and
 796 370 denitrification as follows:
 797
 798

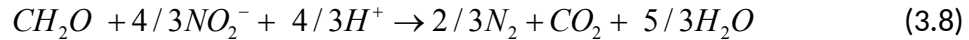
800 371 Oxidative respiration:
 801
 802



803 373 NO_3^- reduction to NO_2^- :
 804
 805



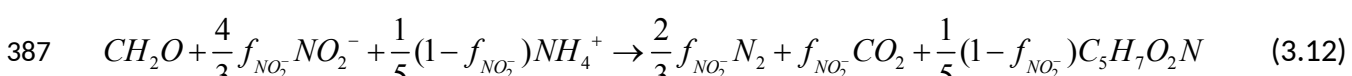
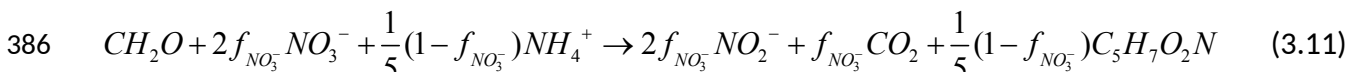
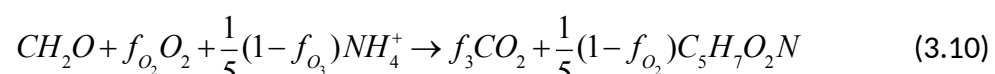
806 375 NO_2^- reduction to N_2 :
 807
 808



809 377 In equation (3.8), multi-stage reduction from NO_2^- to N_2 is lumped into a single reaction by
 810 378 assuming relatively fast dynamics of nitrogen oxide intermediates such as NO and N_2O .
 811
 812 379 Microbial biomass production can be written as follows:
 813
 814



815 381 Microbes obtain energy for growth and maintenance through aerobic or anaerobic respiration
 816 382 depending on what electron acceptors are available in environment. To account for this coupling,
 817 383 each of the energy-producing reactions, equations (3.6) – (3.8), is combined with biomass
 818 384 synthesis reaction, equation (3.9), as follows:
 819
 820



831 388 where f_{O_2} , $f_{NO_3^-}$, and $f_{NO_2^-}$ are parameters that denote the fraction of energy-producing
 832 389 pathway. Due to our focus on simulating carbon and nitrogen flows, H^+ and H_2O are omitted in
 833
 834

841
842
843 390 the equations above. Equations (3.10) - (3.12) share the same electron donor (CH_2O), but involve
844 different electron acceptors (i.e., O_2 for aerobic respiration, NO_3^- and NO_2^- for anaerobic
845 respiration), thus representing three alternative pathways for the production of biomass
846
847 392
848 393 ($C_5H_7O_2N$).
849

850 394 The reactants and products in the simulations include $C_5H_7O_2N$, CO_2 , CH_2O , O_2 , NO_3^- , NO_2^- , and
851 N_2 . Hereafter, we use DOC (dissolved organic carbon), DIC (dissolved inorganic carbon) and
852 BM (biomass) to denote CH_2O , CO_2 and $C_5H_7O_2N$ for simplicity.
853
854

855 397 Dynamic mass balances of key variables in simulation can be written based on stoichiometric
856 equations (3.10) - (3.12) as follows:
857
858

$$399 \quad \frac{d}{dt} \begin{bmatrix} [DOC] \\ [O_2] \\ [NO_3^-] \\ [NO_2^-] \\ [N_2] \\ [DIC] \\ [BM] \end{bmatrix} = \begin{bmatrix} -1 & -1 & -1 \\ -f_{O_2} & 0 & 0 \\ 0 & -2f_{NO_3^-} & 0 \\ 0 & 2f_{NO_3^-} & -4f_{NO_2^-}/3 \\ 0 & 0 & 3f_{NO_2^-}/2 \\ f_{O_2} & f_{NO_3^-} & f_{NO_2^-} \\ (1-f_{O_2})/5 & (1-f_{NO_3^-})/5 & (1-f_{NO_2^-})/5 \end{bmatrix} \begin{bmatrix} r_{O_2} \\ r_{NO_3^-} \\ r_{NO_2^-} \end{bmatrix} [BM] \quad (3.13)$$

870 400 where r_{O_2} , $r_{NO_3^-}$, and $r_{NO_2^-}$ denote microbes' carbon uptake rates through three reaction
871 pathways (equation (3.10) - (3.12)), respectively. Finally, mass balances of BM and DOC are
872 modified to account for biomass degradation and the resulting impact on DOC concentration,
873
874

$$403 \quad \frac{d[BM]}{dt} = \left(\frac{1-f_{O_2}}{5} r_{O_2} + \frac{1-f_{NO_3^-}}{5} r_{NO_3^-} + \frac{1-f_{NO_2^-}}{5} r_{NO_2^-} - k_{deg} \right) [BM] \quad (3.14)$$

$$404 \quad \frac{d[DOC]}{dt} = - \left(r_{O_2} + r_{NO_3^-} + r_{NO_2^-} - 5k_{deg} \right) [BM] \quad (3.15)$$

882 405 where k_{deg} denotes the rate of biomass degradation [1/day].
883
884

885 406 Three biogeochemical reactions considered above can be modeled as being catalyzed by distinct
886 enzymes as follows:
887
888

$$408 \quad r_{O_2} = e_{O_2} r_{O_2}^{kin}, \quad r_{NO_3^-} = e_{NO_3^-} r_{NO_3^-}^{kin}, \quad r_{NO_2^-} = e_{NO_2^-} r_{NO_2^-}^{kin} \quad (3.16)$$

897
 898
 899
 900 where e_{O_2} , $e_{NO_3^-}$, and $e_{NO_2^-}$ denote the relative level of enzymes that catalyze aerobic respiration
 901 and two-step denitrification reactions, respectively, and $r_{O_2}^{kin}$, $r_{NO_3^-}^{kin}$, and $r_{NO_2^-}^{kin}$ are
 902
 903 unregulated reaction rates that can be represented by Monod kinetics, i.e.,
 904
 905

$$906 \quad r_{O_2}^{kin} = k_{O_2} \frac{[DOC]}{K_{d,O_2} + [DOC]} \frac{[O_2]}{K_{a,O_2} + [O_2]} \\ 907 \\ 908 \quad r_{NO_3^-}^{kin} = k_{NO_3^-} \frac{[DOC]}{K_{d,NO_3^-} + [DOC]} \frac{[NO_3^-]}{K_{a,NO_3^-} + [NO_3^-]} \quad (3.17) \\ 909 \\ 910 \\ 911 \\ 912 \quad r_{NO_2^-}^{kin} = k_{NO_2^-} \frac{[DOC]}{K_{d,NO_2^-} + [DOC]} \frac{[NO_2^-]}{K_{a,NO_2^-} + [NO_2^-]} \\ 913 \\ 914$$

915 While enzyme levels are determined by solving dynamic enzyme balance equations in the
 916 original formulation of the cybernetic modeling, they can be determined through a direct linkage
 917 to the cybernetic control laws [Young and Ramkrishna, 2007]:
 918
 919

$$920 \quad e_{O_2} = \frac{r_{O_2}^{kin}}{r_{O_2}^{kin} + r_{NO_3^-}^{kin} + r_{NO_2^-}^{kin}}, \quad e_{NO_3^-} = \frac{r_{NO_3^-}^{kin}}{r_{O_2}^{kin} + r_{NO_3^-}^{kin} + r_{NO_2^-}^{kin}}, \quad e_{NO_2^-} = \frac{r_{NO_2^-}^{kin}}{r_{O_2}^{kin} + r_{NO_3^-}^{kin} + r_{NO_2^-}^{kin}} \quad (3.18) \\ 921 \\ 922 \\ 923$$

924 The above equation implies that microbes control the synthesis of enzymes in proportion to their
 925 relative contribution to a chosen objective (i.e., the carbon uptake rate). This formulation enables
 926 the model to simulate the dynamic shift among three electron acceptors (i.e., O_2 , NO_3^- and NO_2^-)
 927 without having to rely on empirical inhibitive kinetics.
 928
 929

930 Key parameters of denitrification, including $f_{NO_3^-}$, $f_{NO_2^-}$, $k_{NO_3^-}$ and $k_{NO_2^-}$ and k_{deg} , are
 931 determined through model fit to the batch denitrification data [Li et al., 2016], which was
 932 collected using the sediment obtained from the Columbia River hyporheic zone at the US DOE's
 933 Hanford Site. More details of the lab sediment experiments are reported in previous studies [Li et
 934 al., 2016]. Literature data are used for the half saturation constants associated with *DIC* (i.e.,
 935 K_{d,NO_3^-} and K_{d,NO_2^-}) and electron acceptors (i.e., K_{a,NO_3^-} and K_{a,NO_2^-}) [Rittmann and McCarty,
 936 2001; Yan S. et al., 2016]. Parameters associated with oxidative respiration are determined by
 937 assuming the relation to anaerobic respiration, i.e., 1) oxidative respiration is energetically more
 938 favorable than NO_3^- reduction (i.e., $f_{O_2} = f_{NO_3^-} / 3$, $k_{O_2} = 3k_{NO_3^-}$) and 2) half saturation constants
 939 are the same (i.e., $K_{d,O_2} = K_{d,NO_3^-}$, $K_{a,O_2} = K_{a,NO_3^-}$). This parameter setting leads to the sequential
 940
 941
 942
 943
 944
 945
 946
 947
 948
 949
 950
 951
 952

utilization of three alternative electron acceptors, i.e., O_2 , NO_3^- , NO_2^- , and in batch reactor simulation. Model parameters used for simulations here are summarized in Table 4 and are based on fitting model results to the experimental data, which shows good agreement [Song H.-S. et al., 2017].

Table 4. Parameter values of the biogeochemical model used to simulate the interaction between environment and microbial growth through aerobic respiration and denitrification.

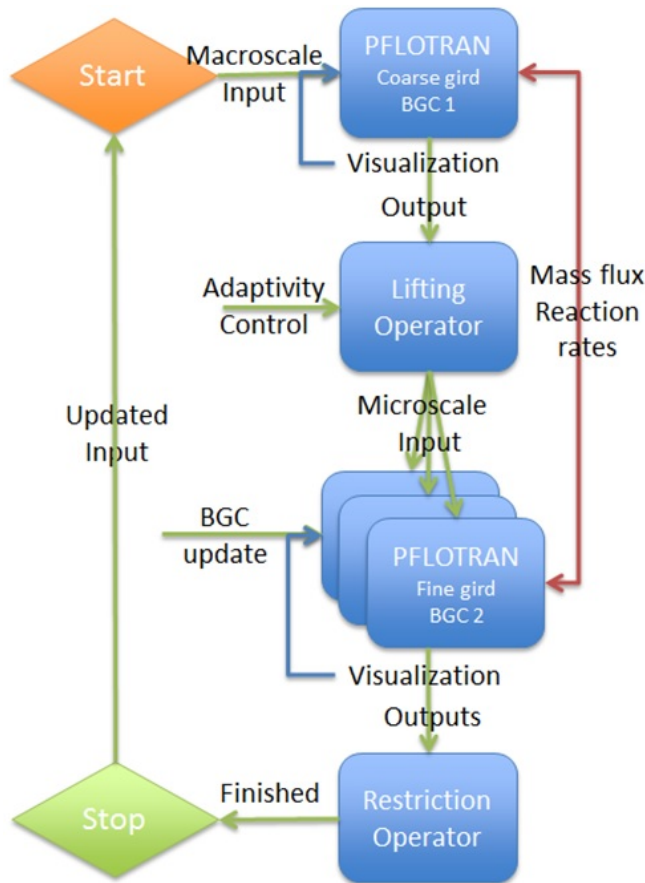
Parameter	Aerobic respiration	NO_3^- reduction	NO_2^- reduction
Fractional of energy-producing pathway [-]	$f_{O_2} = 0.217$	$f_{NO_3^-} = 0.65$	$f_{NO_2^-} = 0.99$
Reaction rate constant [mmol/mmol BM/day]	$k_{O_2} = 84.78$	$k_{NO_3^-} = 28.26$	$k_{NO_2^-} = 23.28$
Half saturation constant of electron donor [mM]	$K_{d,O_2} = 0.25$	$K_{d,NO_3^-} = 0.25$	$K_{d,NO_2^-} = 0.25$
Half saturation constant of electron acceptor [mM]	$K_{a,O_2} = 0.001$	$K_{a,NO_3^-} = 0.001$	$K_{a,NO_2^-} = 0.004$
Biomass degradation rate [1/day]		$k_{deg} = 0.242$	

3. Hybrid Multiscale Modeling Approach

3.1. A loose-coupling framework

The hybrid multiscale modeling framework follows the loose-coupling method presented in Scheibe et al. [2015b; 2015c]. In the current framework, the computational domain is divided into hierarchical macroscale and microscale subdomains that are simulated using different models. The at-scale simulations are conducted sequentially and loosely-coupled by customized scripts. In the current study, as shown in Figure 2 and Table 1, the microscale subdomain (alluvial layer) is simulated using the Richards equation with fine grid resolution and the cybernetic BGC model [Song H.-S. et al., 2017], and the macro-scale subdomain including the Hanford and Ringold formations are simulated using the Richards equation with coarse grid resolution and the BGC model developed by Gu et al. [2012]. The concept of the loose-coupling method is to use script-based functional operators to perform numerical upscaling/downscaling, exchange data (file based) and convert between input and output files from at-scale simulators

1009
1010
1011 452 where the two domains overlap. Advantages of the loose-coupling method include (1) it does not
1012 453 require modification of the at-scale simulators and (2) ease of programming. Potential
1013 454 disadvantages are 1) numerical errors or instabilities introduced by the sequential coupling, and
1014 455 2) inefficiencies introduced by passing data through I/O files rather than direct message passing.
1015 456 The workflow of the loose-coupling framework for the current application is presented in Figure
1016 457 5, which includes the following steps:
1017
1018 458 1. The macroscale simulator (PFLOTRAN) is applied over the full computational domain.
1019 459 Flow and reactive transport simulation using BGC model by Gu et al. [2012] are
1020 460 executed for a specified period of time. Configuration files describing the initial model
1021 461 configuration (initial condition, boundary condition and parameters) are provided to
1022 462 start the simulation at the beginning of the workflow.
1023
1024 463 2. A serial python script –Lifting Operator (LO) –executes the downscaling step (interface
1025 464 coupling and model updating) and constructs microscale simulator (PFLOTRAN) input
1026 465 files. The LO script provides algorithms to reconstruct initial conditions for micro-scale
1027 466 subdomains based on macro-scale quantities from Step 1. Since the size of the micro-
1028 467 scale subdomain is fixed in the current application, no adaptivity control (to
1029 468 dynamically determine the micro-scale subdomains) is needed.
1030
1031 469 3. The microscale simulator (PFLOTRAN) is then applied only to the alluvial layer
1032 470 subdomain with the cybernetic BGC model [Song H.-S. et al., 2017] and finer grids, and
1033 471 is executed for the same period of time as the previous macroscale simulation.
1034
1035 472 4. A serial python script – Restriction Operator (RO) –performs numerical upscaling
1036 473 (interface coupling and averaging) and constructs macroscale input files for the next
1037 474 time step based on outputs from the microscale simulations.
1038
1039 475 5. Repeat the procedure until the entire simulation period is completed.
1040
1041
1042
1043
1044
1045
1046
1047
1048
1049
1050
1051 476
1052
1053
1054
1055
1056
1057
1058
1059
1060
1061
1062
1063
1064



477
478 Figure 5. Swift-managed flowchart and execution for the current application
479

500 3.2. *Coupling strategies*

501 The challenge in all hybrid methods based on physical domain decomposition is how to ensure
502 consistency between the macroscale and microscale subdomains [Scheibe et al., 2015a;
503 Mehmani and Balhoff 2015]. For flow and reactive transport problems, it is critical to ensure
504 consistency of flow and concentrations of multiple chemical species and their flux at the
505 interface (in this case, the bottom boundary of the alluvium layer). There are two critical issues
506 for coupling in the current application: (1) multi-grid matching and (2) consistency of the BGC
507 models. Since the heterogeneity and unique HBGC processes in the alluvium (microscale
508 subdomain) require simulations with higher resolution, we refine the grids in the microscale
509 subdomain relative to the coarser grids used in the macroscale subdomain. Different ratios of
510 grid resolutions (macro- to micro-) were tested: 1:1, 1:0.5 and 1:0.25. To match the values
511 (velocity, concentration and their fluxes) on the nodes of the nested grids, the loose-coupling
512

1121
1122
1123
1124 492 method uses an interpolation/extrapolation scheme for the dependent variable along the interface.
1125 493 From macro-scale to micro-scale subdomain, the nodal values of the coarse grid are distributed
1126 494 evenly to the fine nodes. On the other hand, the nodal values simulated on the fine grids are
1127 495 averaged to coarse grids. A prediction-correction procedure is enforced in each time step. For
1128 496 example, for flow simulations, at the beginning of each time step, we use the velocity from the
1129 497 last time step at the interface. Thereafter the flow and transport equations in the macro-scale
1130 498 subdomain can be solved. Then we pass the interfacial pressure to the micro-scale subdomain,
1131 499 and solve the governing equations to correct the micro-scale velocity. We repeat this procedure
1132 500 iteratively until convergence. The same procedure is conducted for transport simulations. The
1133 501 two BGC models presented in Section 2.4 are different in terms of species and reaction rates. In
1134 502 Gu et al. [2012], the species (reactants and products) include H^+ , CO_2 , CH_2O , O_2 , NO_3^- and N_2 .
1135 503 In the cybernetic model [Song et al., 2017], the reactants and products being monitored in the
1136 504 simulations include $C_5H_7O_2N$, CO_2 , CH_2O , O_2 , NH_4^+ , NO_3^- , NO_2^- , and N_2 . The number of
1137 505 reactions and species are slightly different in two models. For variable data exchange, we only
1138 506 pass those that co-exist in both models. The reaction rates are calculated in each time step, then
1139 507 passed and updated between scales.
1140
1141
1142
1143
1144
1145
1146
1147
1148

1149 508 3.3. *Simulation cases*

1150 509 To validate and apply the above Swift-managed workflow to the 2D modeling domain, we set up
1151 510 a series of simulation cases using increasingly complex scenarios. A list of the cases is
1152 511 summarized in Table 5.
1153
1154

1155 512 1. Case 1 is designed to validate that the multiscale coupling algorithm is working
1156 513 correctly. In this case, we compare results from the hybrid multiscale simulation
1157 514 (including multiple nested grid ratios) with equivalent single-scale (single-domain)
1158 515 simulations using a uniform grid resolution, homogeneous properties and one BGC
1159 516 model (Gu et al., 2012). Since both the multiscale and single-scale models use the same
1160 517 property distributions and BGC model, the only difference is the multiscale coupling
1161 518 and subgrid resolution, and all solutions should be comparable.
1162
1163 2. Following successful validation, Case 2 simulations are designed to evaluate the
1164 519 potential impacts of sub-grid heterogeneity within the alluvial layer only. We apply
1165 520
1166
1167
1168
1169
1170
1171
1172
1173
1174
1175
1176

1177
 1178
 1179 521 several realizations of the statistical heterogeneity model (Section 2.2) to the alluvium
 1180 522 only (microscale subdomain) and compare with the homogeneous case (Case 1).
 1181
 1182 523 3. Case 3 is designed to evaluate the potential impacts of applying an alternative and more
 1183 524 complex BGC model in the alluvium layer. The BGC model of Song H.-S. et al. [2017]
 1184 525 is applied in the alluvium while maintaining use of the Gu et al. [2012] BGC model in
 1185 526 the larger domain. Again, results are compared to Case 1 which uses the Gu et al. [2012]
 1187 527 model everywhere.
 1188
 1189 528 4. Case 4 applies the full combination of nested multiscale grids, heterogeneities in all
 1190 529 formations, and different BGC model in the alluvial layer. This reflects the full level of
 1191 530 complexity that is enabled by the hybrid multiscale coupling, and the results are
 1192 531 evaluated to determine whether representing this level of complexity could reveal
 1193 532 different behaviors from the simpler cases above.
 1194
 1195
 1196
 1197
 1198
 1199
 1200 533

534 Table 5. A list of simulation cases

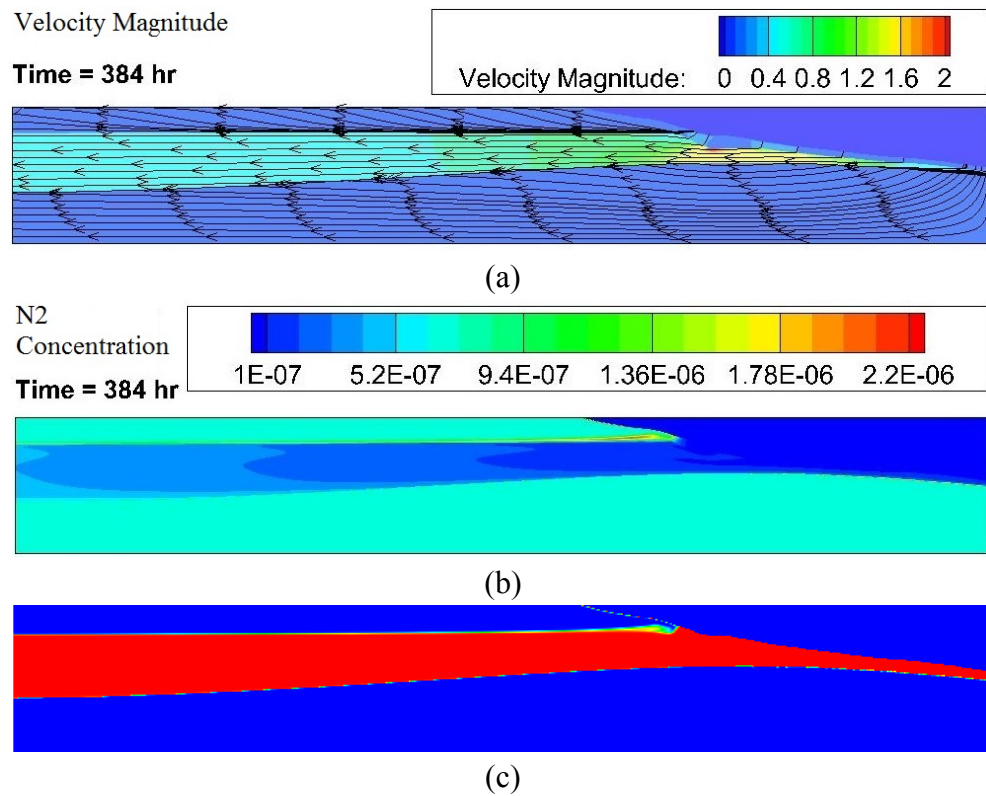
Scale\Case	Case 1	Case 2	Case 3	Case 4
Macro-scale	Coarse/fine grid Homogeneous BGC model 1	Coarse grid Homogeneous BGC model 1	Coarse grid Homogeneous BGC model 1	Coarse grid Homogeneous BGC model 1
Micro-scale	Coarse/fine grid Homogeneous BGC model 1	Fine grid Heterogeneous BGC model 1	Fine grid Homogeneous BGC model 2	Fine grid Heterogeneous BGC model 2

535
 1218 536 **4. Results**

1220 537 *4.1. Case 1: Validation*

1223 538 The hybrid multiscale model was applied to simulate HBGC processes in the 2D domain over a
 1224 539 2500 hr time period. The instantaneous velocity (with streamlines) and reaction product (N_2)
 1225 540 species concentration contour plots at a selected time (384 hours) are shown in Figure 6.
 1227 541 Intrusion of river water into the various subsurface formations is clearly evident. The

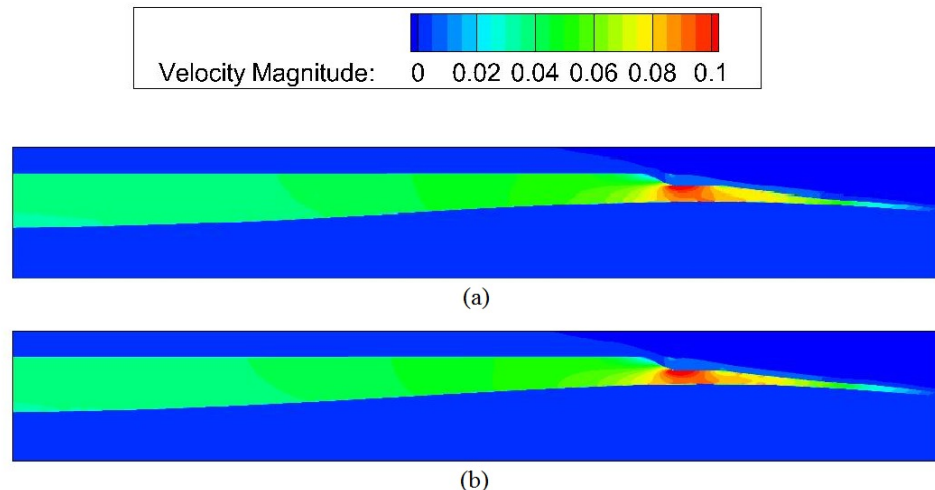
1233
1234
1235 542 geostratigraphic formations strongly impact the flow paths, with the fastest flow paths occurring
1236 543 in the high-permeability Hanford formation. The purpose of Case 1 is to validate the multiscale
1238 544 coupling methodology by comparing results to equivalent single-scale simulations. For this case,
1239 545 a uniform fine (high-resolution 0.05 m horizontal x 0.025 m vertical) grid was used for the
1241 546 single-scale model, whereas the multiscale model used variable nested grids.
1243 547



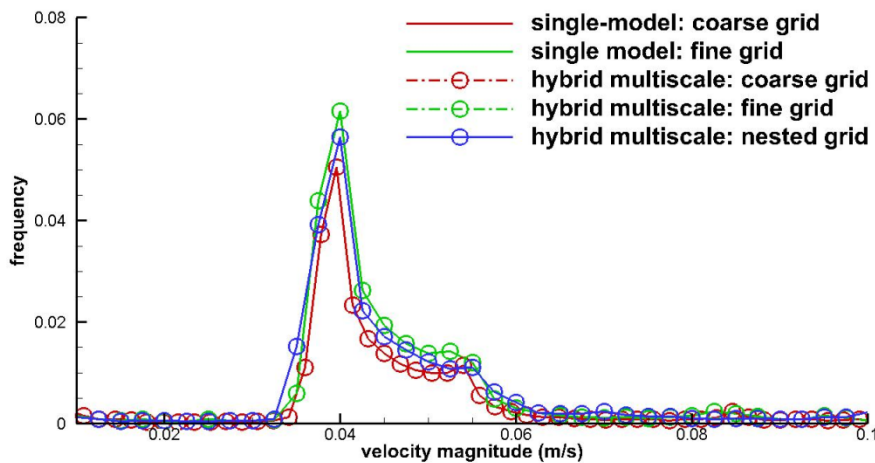
1251 548 Figure 6. Instantaneous contour plots of (a) velocity magnitude, (b) concentrations of N_2 and (c)
1252 549 tracer.

1262 550
1263 551
1264 552
1265 553
1266 554 Figures 7-9 present the comparisons from different perspectives. Instantaneous contour plots of
1267 555 velocity magnitude are shown in Figure 7, which shows minimal differences between the single-
1268 556 scale and multi-scale simulations. To further quantify the results, velocity distributions
1269 557 (histograms) are shown in Figure 8 for a series of simulations with different computational grids
1270 558 (Figure 8). The hybrid multiscale result with a uniformly fine grid is indistinguishable from that
1271 559 of the equivalent single-scale model, indicating minimal error introduced by the coupling
1272 560 process. Employment of a coarse (0.1 m horizontal x 0.05 m vertical) grid everywhere introduces
1273 561 errors of up to 6%. The nested grid used in the multiscale simulation (coarse-to-fine ratio equals
1274 562
1275 563
1276 564
1277 565
1278 566
1279 567
1280 568
1281 569
1282 570
1283 571
1284 572
1285 573
1286 574
1287 575
1288 576

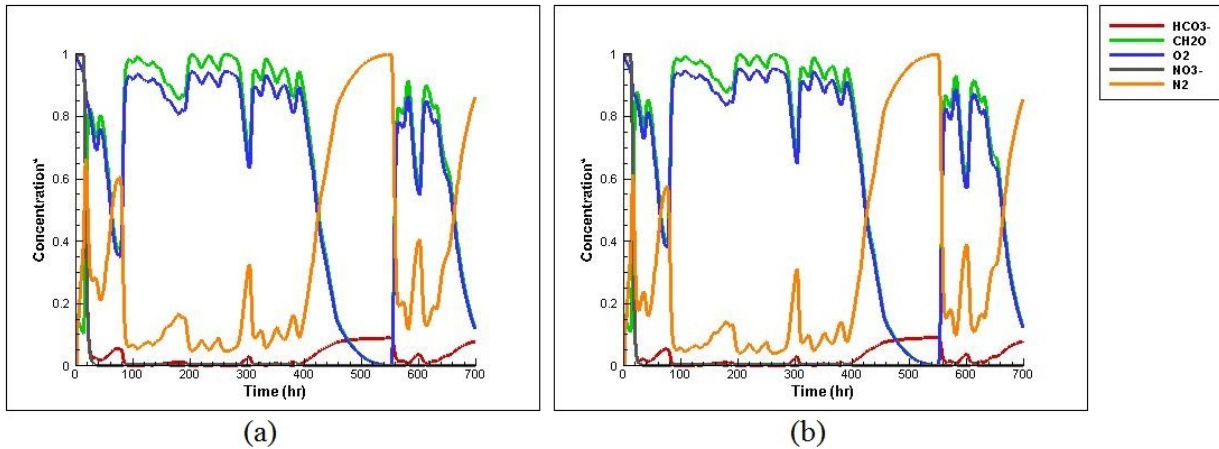
1289
1290
1291 565 to 0.25) provides results that are more accurate than the coarse grid, but still have small errors
1292 566 relative to the uniform fine grid. This is expected from the loosely-coupled multiscale method,
1293 567 and represents the tradeoff between accuracy and computational demand. In cases where a
1294 568 uniform fine grid is not computationally feasible, the multiscale method provides higher
1295 569 accuracy than a uniform coarse grid, but with a relatively modest increase in computational
1296 570 demand. To evaluate impacts on predictions of biogeochemical reactions, multiple species
1300 571 concentration histories at one of the hypothetical observation locations (Well 2M in the alluvium
1302 572 in Figure 2) are presented in Figure 9. Again the results obtained from the single- and multi-scale
1303 573 simulations (based on uniform fine grids and BGC model from Gu et al. 2012) are
1305 574 indistinguishable, which validates the loose coupling of reactive transport.
1307 575



576
577 Figure 7. Comparisons of velocity magnitude contour plots ($t = 384$ hr): (a) single-scale
578 simulation using uniform fine grids; (b) hybrid multi-scale simulation using nested grids.
579



580
581 Figure 8. Comparisons of velocity histograms between single- and multi-scale models.
582

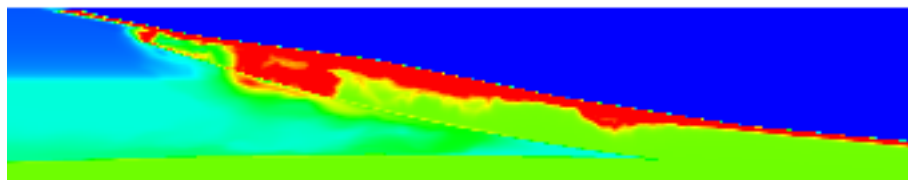


583
584 Figure 9. Comparisons of species concentration time histories (using the same setup) between (a)
585 single-scale model and (b) hybrid multi-scale model.

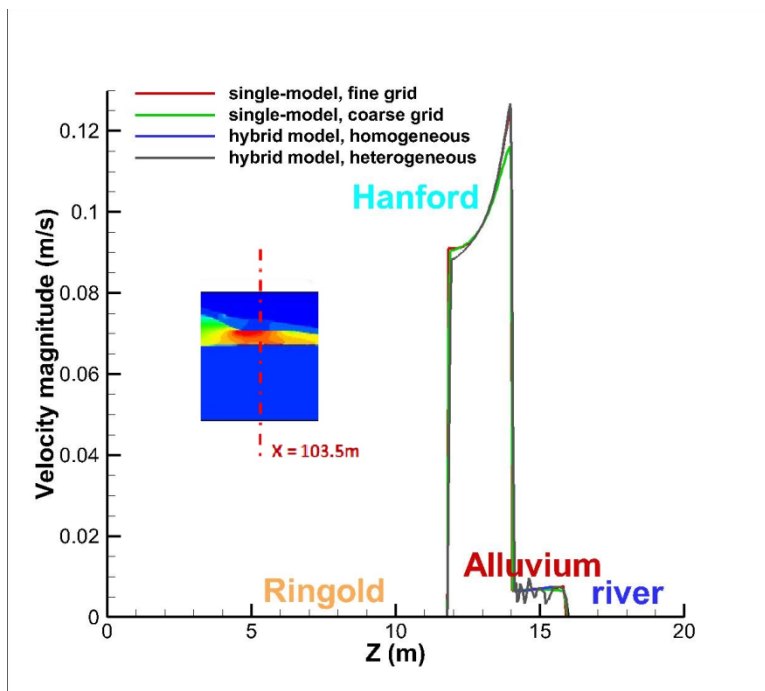
586
587 Finally, we present the results of computing cost in terms of CPU hrs (Table 5). For uniform
588 (fine or coarse) grids, the hybrid simulations use more CPU time than the corresponding single-
589 scale models due to computational overhead associated with model coupling and data/file
590 exchange. However, for the nested grid in multiscale hybrid simulations, the computing cost was
591 significantly reduced relative to single-scale simulations on uniform fine grids. These results
592 demonstrate that the loosely-coupled hybrid multiscale simulation method is a feasible approach
593 for investigation of the impacts of detailed processes and property distributions within
594 microscale subdomains.

1401
1402
1403
1404
1405 595 4.2. *Case 2: Impact of micro-scale heterogeneity*

1406
1407 Having established confidence in the numerical coupling algorithm based on Case 1
1408 comparisons, we now apply our hybrid multiscale model approach to more complex cases. We
1409 consider these additional cases as numerical experiments to evaluate the potential impact of
1410 small-scale heterogeneity and complex biogeochemistry within the alluvial layer. Case 2 tests the
1411 potential impacts of permeability heterogeneity in the alluvial layer by replacing the
1412 homogeneous properties used in Case 1 with heterogeneous distributions (using a
1413 geostatistically-generated realization). Figure 10 shows the altered flow field in the alluvium and
1414 associated velocity profiles along a selected transect as shown in the figure. Comparisons
1415 between homogeneous and heterogeneous cases are provided along the transect (red dashed
1416 line). While the overall results are similar for all cases, variable velocities are observed in the
1417 alluvium layer for the multiscale case, indicating that the microscale heterogeneity impacts flow
1418 fields within the microscale subdomain but not in the macroscale domain. Figure 11 shows the
1419 time history of the considered biogeochemical species at hypothetical observation location 2M
1420 (Figure 2). In comparison to Figure 9 (Case 1), the overall trends are similar but there are some
1421 significant differences, suggesting that physical heterogeneity in the alluvium alone can impact
1422 the system biogeochemistry through formation of preferential flow paths and low-flow zones.
1423
1424 613



(a)



(b)

Figure 10. Case 2: (a) distribution of river water (as a tracer) within the alluvium at a selected time point ($t = 384$ hr), showing the impacts of alluvial heterogeneity; (b) comparisons among velocity magnitude profiles (along the red dashed line across the domain) for single-scale and multiscale models on different grids and with homogeneous and heterogeneous alluvium properties.

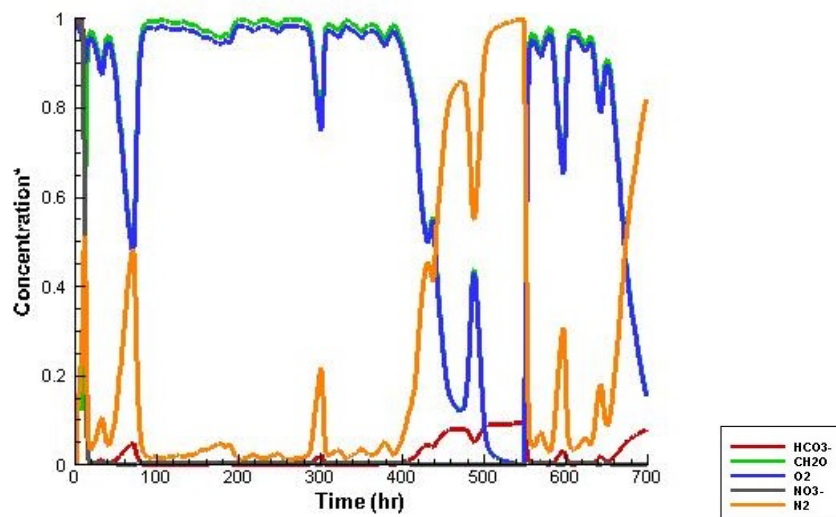
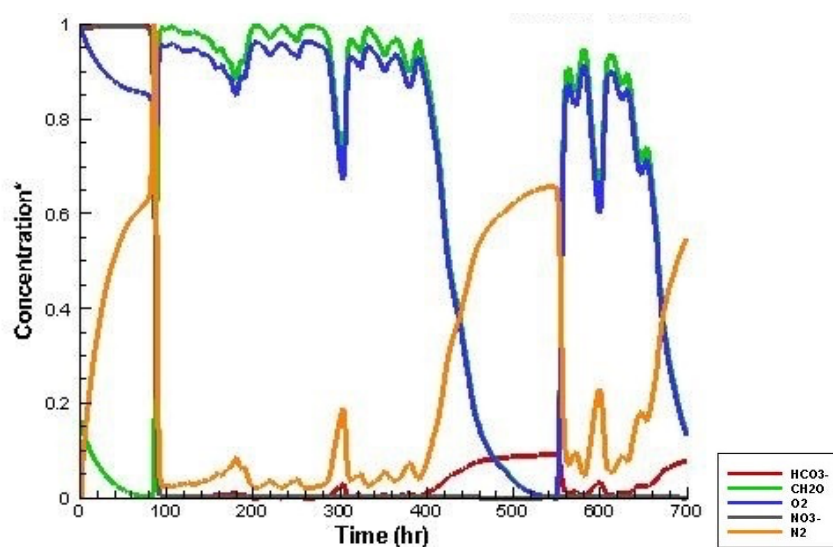


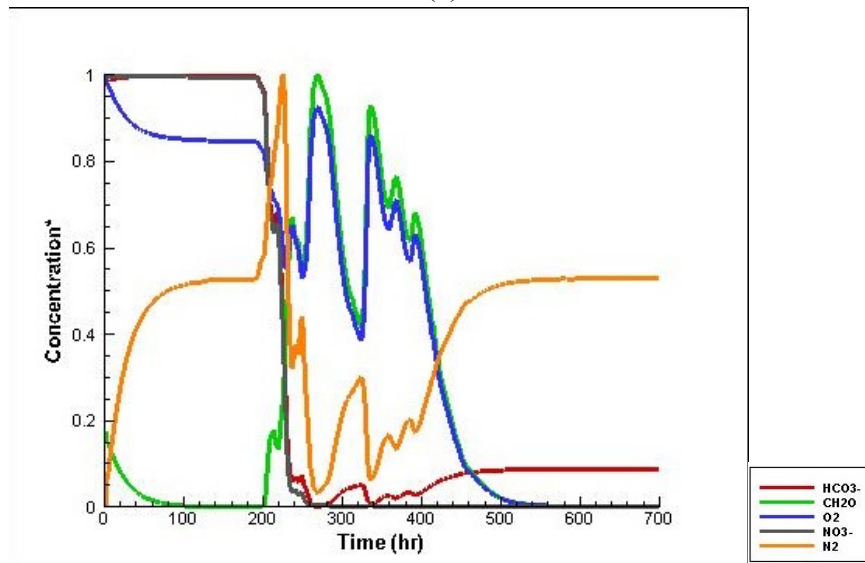
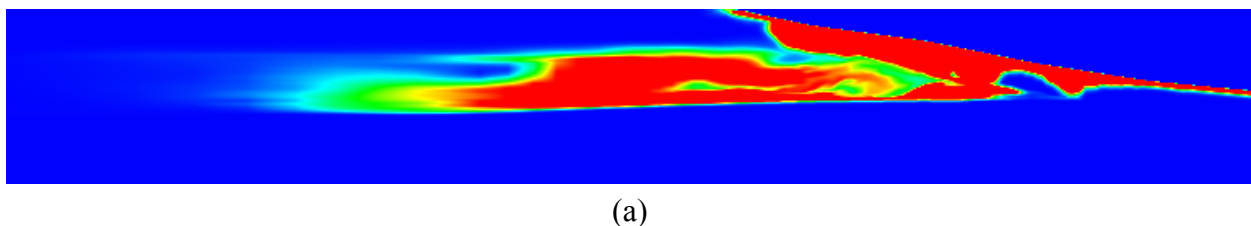
Figure 11. Impact of small-scale permeability heterogeneity in the alluvium on biogeochemical reaction outcomes; compare to Figure 9.

1513
 1514
 1515 628 4.3. *Case 3: Impact of alternative BGC model in the alluvium*
 1516
 1517 629 In Case 3, we employ the more complex biogeochemical model of Song H.-S. et al. [2017],
 1518 developed specifically for alluvial sediments, in the microscale subdomain while keeping the
 1519 more general model of Gu et al. [2012] used in the macro-scale subdomain. Since there are two
 1520 pathways in the model by Song H.-S. et al. [2017], there exist additional species and
 1521 intermediate products that are not simulated in the macroscale domain. This inconsistency
 1522 induces some potential numerical instability in the loose coupling algorithm. For comparison
 1523 purposes, we consider only those species simulated in both biogeochemical models. Figure 12
 1524 again shows the time histories of the species concentrations at hypothetical observation point
 1525 2M. Comparison to Case 1 results (Figure 9) indicate significantly lower simulated
 1526 concentrations of N_2 (reaction product) among other differences, which suggests that the
 1527 application of a more complex reaction network within the biogeochemically active alluvial layer
 1528 can lead to significant differences in model prediction. However, since we do not have direct
 1529 observational information for comparison, we cannot confidently state that this prediction is in
 1530 fact better. What is clear is that the multiscale hybrid approach enables the use of more complex
 1531 representations of biogeochemistry (Case 3) and physical heterogeneity (Case 2) which could
 1532 have significant impacts on model predictions. Additional model testing and experimental data
 1533 are needed to confirm the significance of these differences.
 1534
 1535 640
 1536 641
 1537 642
 1538 643
 1539 644
 1540 645
 1541
 1542
 1543



1569
1570
1571 651 4.4. *Case 4: A complete simulation*
1572

1573 652 This final case combines the complexities of Cases 2 and 3, and in addition incorporates a
1574 653 realization of physical heterogeneity (hydraulic conductivity) in the Hanford and Ringold
1575 654 formations (macroscale domain). Figure 13a shows a snapshot of tracer (river water) distribution
1576 655 at a selected time ($t = 276$ hr), and Figure 13b shows the corresponding time history of
1577 656 biogeochemical species at the hypothetical observation point 2M. The complex flow pattern
1578 657 interacts with the biogeochemical processes (mostly in the alluvial layer) to create transient
1579 658 species behaviors that differ significantly from the homogeneous scenarios (Case 1). Again,
1580 659 additional model testing and experimental data are needed to confirm the significance of these
1581 660 differences. However, our numerical experiments demonstrate that multiscale physical
1582 661 heterogeneity and complexity of the biogeochemical reaction model are key factors that can
1583 662 strongly impact predictions of hydrobiogeochemical processes in the GSIZ.
1584
1585
1586
1587
1588
1589
1590
1591 663



1616 668 Figure 13. Case 4: (a) instantaneous contour plot of tracer transport ($t = 276$ hr); (b) BGC species
1617 669 concentration time histories.
1618
1619
1620
1621
1622
1623
1624

1625
1626
1627
671 **5. Summary and Conclusions**
1628

1629
1630
1631 We used a hybrid multiscale modeling approach to simulate hydrologic-biogeochemical
1632 processes (HBGC) in the groundwater-surface water interaction zone (GSIZ) at the US DOE
1633 Hanford 300A site. A 2D modeling domain [Song X. et al., 2017] was studied and decomposed
1634 into macroscale and microscale subdomains based on the spatial configuration of
1635 hydrogeological formations [Hou et al., 2016]. Enhanced biogeochemical activity associated
1636 with groundwater-river water exchange has been observed in a heterogeneous thin alluvial layer
1637 that is adjacent to the river. Resolution of these processes was enabled by utilizing a fine grid and
1638 complex biogeochemical model in the microscale domain, coupled to a coarser grid and simpler
1639 biogeochemical model in the macroscale domain. A hybrid multiscale method was implemented
1640 in a script-based high-performance computing workflow to loosely couple microscale and
1641 macroscale models, both implemented using the same reactive transport simulator, through
1642 upscaling/downscaling methods and file-based data exchange.
1643
1644

1645
1646
1647
1648
1649 The hybrid multiscale model algorithm was successfully validated by comparing results to a
1650 single-scale simulation with uniformly fine grid, homogeneous facies properties and uniform
1651 BGC models. Comparisons demonstrate that the hybrid multiscale simulation approach provides
1652 greater process fidelity than a coarsely-resolved single-scale model while maintaining higher
1653 computational efficiency than a finely-resolved single-scale model. A series of numerical
1654 experiments demonstrated potential impacts of incorporating microscale heterogeneity and
1655 complex biogeochemistry on model predictions; further testing and validation against
1656 experimental results are needed to confirm these outcomes. The use of stochastic simulation
1657 methods to represent heterogeneous properties also can enable future study of model
1658 uncertainties associated with microscale heterogeneity.
1659
1660

1661
1662
1663
1664
1665
1666 Our results demonstrate that hybrid multiscale models can be successfully implemented in field-
1667 scale simulations with complex subsurface sediment structures and complicated HBGC
1668 processes. The 2D model system used here for method demonstration and testing does not
1669 require the computational efficiency of the multiscale approach, but the same method can easily
1670 be extended to 3D domains of much larger size for which this efficiency will be required. Further
1671 developments of the hybrid multiscale models, especially refinement of the coupling methods,
1672
1673
1674
1675
1676
1677
1678
1679
1680 are needed to ensure robustness and generalizability. Research is continuing in (1) development

1681
1682
1683 701 of a generalized hybrid multiscale modeling framework using a universal coupling interface and
1684 702 (2) intercomparison and community benchmarking of alternative hybrid multiscale modeling
1685 703 approaches.
1686
1687

1688 704 **Acknowledgement**
1689
1690

1691 705 This research was supported by the U. S. Department of Energy (DOE) Office of Biological and
1692 706 Environmental Research (BER), Subsurface Biogeochemical Research (SBR) program, through
1693 707 the PNNL SBR Scientific Focus Area project and the Interoperable Design of Extreme-scale
1694 708 Application Software (IDEAS) project. Computations described here were performed at the
1695 709 National Energy Research Supercomputing Center (NERSC), which is supported by the DOE
1696 710 Office of Science under contract DE-AC02-05CH11231.
1697 711

1698 712 **References**
1699
1700

713 [1] Balhoff MT, SG Thomas, MF Wheeler. Mortar coupling and upscaling of pore-scale models.
714 Computational Geosciences. 12 (2007) 15-27, doi: 10.1007/s10596-007-9058-6.
715 [2] Barajas-Solano DA, AM Tartakovsky. Hybrid Multiscale Finite Volume Method for Advection-
716 Diffusion Equations Subject to Heterogeneous Reactive Boundary Conditions. Multiscale Modeling &
717 Simulation. 14 (2016) 1341-76, doi: 10.1137/15m1022537.
718 [3] Bardini L, F Boano, MB Cardenas, AH Sawyer, R Revelli, L Ridolfi. Small-scale permeability
719 heterogeneity has negligible effects on nutrient cycling in streambeds. Geophysical Research Letters. 40
720 (2013) 1118-22, doi: 10.1002/grl.50224.
721 [4] Battiatto I, DM Tartakovsky, AM Tartakovsky, TD Scheibe. Hybrid models of reactive transport in
722 porous and fractured media. Advances in Water Resources. 34 (2011) 1140-50, doi:
723 10.1016/j.advwatres.2011.01.012.
724 [5] Bencala KE. Hyporheic zone hydrological processes. Hydrological Processes. 14 (2000) 2797-8.
725 [6] Bjornstad BN, PD Thorne, BA Williams, GV Last, GS Thomas, MD Thompson, et al. Hydrogeologic
726 Model for the Gable Gap Area, Hanford Site. Pacific Northwest National Laboratory, Richland,
727 Washington, 2010.
728 [7] Boano F, JW Harvey, A Marion, AI Packman, R Revelli, L Ridolfi, et al. Hyporheic flow and
729 transport processes: Mechanisms, models, and biogeochemical implications. Reviews of Geophysics. 52
730 (2014) 603-79, doi: 10.1002/2012RG000417.
731 [8] Brunke M, T Gonser. The ecological significance of exchange processes between rivers and
732 groundwater. Freshwater Biology. 37 (1997).
733 [9] Brunner P, CT Simmons, PG Cook, R Therrien. Modeling surface water-groundwater interaction with
734 MODFLOW: some considerations. Ground Water. 48 (2010) 174-80, doi: 10.1111/j.1745-
735 6584.2009.00644.x.
736 [10] Cardenas MB. Hyporheic zone hydrologic science: A historical account of its emergence and a
737 prospectus. Water Resources Research. 51 (2015) 3601-16, doi: 10.1002/2015WR017028.
738 [11] Cass A, GS Campbell, TI Jones. Hydraulic and Thermal Properties of Soil Samples from the Buried
739 Waster Test Facility. Pacific Northwest National Laboratory, Richland, Washington, 1981.
740 [12] Chen X, MB Cardenas, L Chen. Three-dimensional versus two-dimensional bed form-induced
741 hyporheic exchange. Water Resources Research. 51 (2015) 2923-36, doi: 10.1002/2014WR016848.
742
743
744
745
746
747
748
749
750
751
752
753
754
755
756
757
758
759
760
761
762
763
764
765
766
767
768
769
770
771
772
773
774
775
776
777
778
779
780
781
782
783
784
785
786
787
788
789
790
791
792
793
794
795
796
797
798
799
800
801
802
803
804
805
806
807
808
809
810
811
812
813
814
815
816
817
818
819
820
821
822
823
824
825
826
827
828
829
830
831
832
833
834
835
836
837
838
839
840
841
842
843
844
845
846
847
848
849
850
851
852
853
854
855
856
857
858
859
860
861
862
863
864
865
866
867
868
869
870
871
872
873
874
875
876
877
878
879
880
881

1737
1738
1739
1740 [742] [13] Davis JM, JL Wilson, FM Phillips, MB Gotkowitz. Relationship between fluvial bounding surfaces
1741 and the permeability correlation structure. *Water Resources Research*. 33 (1997) 1843-54, doi:
1742 10.1029/97wr01003.
1743 [745] [14] Di Federico V, SP Neuman. Scaling of random fields by means of truncated power variograms and
1744 associated spectra. *Water Resources Research*. 33 (1997) 1075-85, doi: 10.1029/97wr00299.
1745 [747] [15] Dobermann A, P Goovaerts, HU Neue. Scale-Dependent Correlations among Soil Properties in Two
1746 Tropical Lowland Rice Fields. *Soil Science Society of America Journal*. 61 (1997) 1483-96.
1747 [749] [16] Doussan C, G Poitevin, E Ledoux, M Detay. River bank filtration: modeling of the changes in water
1748 chemistry with emphasis on nitrogen species. *Journal of Contaminant Hydrology*. 25 (1997).
1749 [751] [17] E W, B Engquist, Z Huang. Heterogeneous multiscale method: A general methodology for
1750 multiscale modeling. *Physical Review B*. 67 (2003) 092101, doi: 10.1103/PhysRevB.67.092101.
1751 [753] [18] Findlay S. Importance of surface-subsurface exchange in stream ecosystems: The hyporheic zone.
1752 *Limnology and Oceanography*. 40 (1996) 159-64.
1753 [755] [19] Fleckenstein JH, S Krause, DM Hannah, F Boano. Groundwater-surface water interactions: New
1754 methods and models to improve understanding of processes and dynamics. *Advances in Water Resources*.
1755 33 (2010) 1291-5, doi: 10.1016/j.advwatres.2010.09.011.
1756 [758] [20] Fox A, F Boano, S Arnon. Impact of losing and gaining streamflow conditions on hyporheic
1757 exchange fluxes induced by dune-shaped bed forms. *Water Resources Research*. 50 (2014), doi:
1758 10.1002/2013WR014668.
1759 [761] [21] Frei S, KH Knorr, S Peiffer, JH Fleckenstein. Surface micro-topography causes hot spots of
1760 biogeochemical activity in wetland systems: A virtual modeling experiment. *Journal of Geophysical
1761 Research: Biogeosciences*. 117 (2012) n/a-n/a, doi: 10.1029/2012jg002012.
1762 [764] [22] Fritz BG, EV Arntzen. Effect of rapidly changing river stage on uranium flux through the hyporheic
1763 zone. *Ground Water*. 45 (2007) 753-60, doi: 10.1111/j.1745-6584.2007.00365.x.
1764 [766] [23] Fritz BG, NP Kohn, TJ Gilmore, D McFarland, EV Arntzen, RD Mackley, et al. Investigation of the
1765 Hyporheic Zone at the 300 Area, Hanford Site. Pacific Northwest National Laboratory, Richland,
1766 Washington, 2007.
1767 [769] [24] Gelhar LW. Stochastic Subsurface Hydrology from Theory to Applications. *Water Resources
1768 Research*. 22 (1986) 135S-45S.
1769 [771] [25] Goovaerts P, R Webster. Scale-dependent Correlation between Topsoil Copper and Cobalt
1770 Concentrations in Scotland. *European Journal of Soil Science*. 45 (1994) 79-95.
1771 [773] [26] Gray WG, CT Miller, BA Schrefler. Averaging Theory for Description of Environmental Problems:
1772 What Have We Learned? *Adv Water Resour*. 51 (2013) 123-38, doi: 10.1016/j.advwatres.2011.12.005.
1773 [775] [27] Gu C, W Anderson, F Maggi. Riparian biogeochemical hot moments induced by stream fluctuations.
1774 *Water Resources Research*. 48 (2012) n/a-n/a, doi: 10.1029/2011wr011720.
1775 [777] [28] Gu C, GM Hornberger, AL Mills, JS Herman, SA Flewelling. Nitrate reduction in streambed
1776 sediments: Effects of flow and biogeochemical kinetics. *Water Resources Research*. 43 (2007) n/a-n/a,
1777 doi: 10.1029/2007wr006027.
1778 [780] [29] Hammond GE, PC Lichtner. Field-scale model for the natural attenuation of uranium at the Hanford
1779 300 Area using high-performance computing. *Water Resources Research*. 46 (2010) n/a-n/a, doi:
1780 10.1029/2009wr008819.
1781 [783] [30] Han B, TA Endreny. Comparing MODFLOW simulation options for predicting intra-meander flux.
1782 *Hydrological Processes*. 28 (2014) 3824-32, doi: 10.1002/hyp.10186.
1783
1784
1785
1786
1787
1788
1789
1790
1791
1792

1793
1794
1795 785 [31] Harvey JW, MN Gooseff. River corridor science: Hydrologic exchange and ecological consequences
1796 786 from bedforms to basins. *Water Resources Research*. 51 (2015) 6893-922, doi: 10.1002/2015WR017617.
1797 787 [32] Ingram GD, IT Cameron, KM Hangos. Classification and analysis of integrating frameworks in
1798 788 multiscale modelling. *Chemical Engineering Science*. 59 (2004) 2171-87, doi: 10.1016/j.ces.2004.02.010.
1799 789 [33] Janssen F, MB Cardenas, AH Sawyer, T Dammrich, J Krietsch, D de Beer. A comparative
1800 790 experimental and multiphysics computational fluid dynamics study of coupled surface-subsurface flow in
1801 791 bed forms. *Water Resources Research*. 48 (2012) n/a-n/a, doi: 10.1029/2012wr011982.
1802 792 [34] Johnson T, R Versteeg, J Thomle, GE Hammond, X Chen, JM Zachara. Four-dimensional electrical
1803 793 conductivity monitoring of stage-driven river water intrusion: Accounting for water table effects using a
1804 794 transient mesh boundary and conditional inversion constraints. *Water Resources Research*. 51 (2015)
1805 795 6177-96, doi: 10.1002/2014wr016129.
1806 796 [35] Kessler AJ, RN Glud, MB Cardenas, M Larsen, MF Bourke, PLM Cook. Quantifying denitrification
1807 797 in rippled permeable sands through combined flume experiments and modeling. *Limnology and
1808 798 Oceanography*. 57 (2012) 1217-32, doi: 10.4319/lo.2012.57.4.1217.
1809 799 [36] Krause S, F Boano, MO Cuthbert, JH Fleckenstein, J Lewandowski. Understanding process
1810 800 dynamics at aquifer-surface water interfaces: An introduction to the special section on new modeling
1811 801 approaches and novel experimental technologies. *Water Resources Research*. 50 (2014) 1847-55, doi:
1812 802 10.1002/2013WR014755.
1813 803 [37] Larned ST, MN Gooseff, AI Packman, K Rugel, SM Wondzell. Groundwater-surface-water
1814 804 interactions: current research directions. *Freshwater Science*. 34 (2015) 92-8, doi: 10.1086/679491.
1815 805 [38] Last GV, EJ Freeman, KJ Cantrell, MJ Fayer, GW Gee, WE Nichols, et al. Vadose zone
1816 806 hydrogeology data package for Hanford assessments. Pacific Northwest National Laboratory, Richland,
1817 807 Washington, 2006.
1818 808 [39] Lautz LK, DI Siegel. Modeling surface and ground water mixing in the hyporheic zone using
1819 809 MODFLOW and MT3D. *Advances in Water Resources*. 29 (2006) 1618-33, doi:
1820 810 10.1016/j.advwatres.2005.12.003.
1821 811 [40] Li M, Y Gao, WJ Qian, L Shi, Y Liu, WC Nelson, et al. Quantification of functional enzyme
1822 812 dynamics and its linkage with biogeochemical process kinetics. *Environmental Microbiology*. under
1823 813 review (2016).
1824 814 [41] Liggett JE, D Partington, S Frei, AD Werner, CT Simmons, JH Fleckenstein. An exploration of
1825 815 coupled surface-subsurface solute transport in a fully integrated catchment model. *Journal of Hydrology*.
1826 816 529 (2015) 969-79, doi: 10.1016/j.jhydrol.2015.09.006.
1827 817 [42] Mayer KU, EO Frind, DW Blowes. Multicomponent reactive transport modeling in variably
1828 818 saturated porous media using a generalized formulation for kinetically controlled reactions. *Water
1829 819 Resources Research*. 38 (2002) 13-1--21, doi: 10.1029/2001wr000862.
1830 820 [43] Mehmani Y, MT Balhoff. Bridging from Pore to Continuum: A Hybrid Mortar Domain
1831 821 Decomposition Framework for Subsurface Flow and Transport. *Multiscale Modeling & Simulation*. 12
1832 822 (2014) 667-93, doi: 10.1137/13092424x.
1833 823 [44] Mehmani Y, MT Balhoff. Mesoscale and Hybrid Models of Fluid Flow and Solute Transport.
1834 824 *Reviews in Mineralogy and Geochemistry*. 80 (2015) 433-59, doi: 10.2138/rmg.2015.80.13.
1835 825 [45] Molins S. Reactive Interfaces in Direct Numerical Simulation of Pore-Scale Processes. *Reviews in
1836 826 Mineralogy and Geochemistry*. 80 (2015) 461-81, doi: 10.2138/rmg.2015.80.14.
1837 827 [46] Moser DP, JK Fredrickson, DR Geist, EV Arntzen, AD Peacock, S-MW Li, et al. Biogeochemical
1838 828 Processes and Microbial Characteristics across Groundwater-Surface Water Boundaries of the Hanford
1839
1840
1841
1842
1843
1844
1845
1846
1847
1848

1849
1850
1851
1852 829 Reach of the Columbia River. *Environmental Science and Technology*. 37 (2003) 5127-34, doi:
1853 830 10.1021/es034457v.
1854 831 [47] Newcomb RC, SG Brown. Evaluation of bank storage along the Columbia River between Richland
1855 832 and China Bar. US Govt, Washington, 1961.
1856 833 [48] Newcomb RC, J Strand, F Frank. Geology and ground-water characteristics of the Hanford
1857 834 Reservation of the US Atomic Energy Commission. US Govt., Washington, 1972.
1858 835 [49] Packman AI, M Salehin, M Zaramella. Hyporheic Exchange with Gravel Beds: Basic Hydrodynamic
1859 836 Interactions and Bedform-Induced Advective Flows. *Journal of Hydraulic Engineering*. 130 (2004), doi:
1860 837 10.1061//ASCE/0733-9429/2004/130:7/647.
1861 838 [50] Peterson RE, BA Williams, RM Smith. Volatile Organic Compound Investigation Results, 300 Area,
1862 839 Hanford Site, Washington. Pacific Northwest National Laboratory, Richland, Washington, 2008.
1863 840 [51] Pinay G, S Peiffer, J-R De Dreuzy, S Krause, DM Hannah, JH Fleckenstein, et al. Upscaling
1864 841 Nitrogen Removal Capacity from Local Hotspots to Low Stream Orders' Drainage Basins. *Ecosystems*.
1865 842 18 (2015) 1101-20, doi: 10.1007/s10021-015-9878-5.
1866 843 [52] Ramkrishna D, H-S Song. Dynamic models of metabolism: Review of the cybernetic approach.
1867 844 *AIChE Journal*. 58 (2012) 986-97, doi: 10.1002/aic.13734.
1868 845 [53] Rittmann BE, PL McCarty. *Environmental Biotechnology: Principles and Applications*. McGraw-
1869 846 Hill, New York, 2001.
1870 847 [54] Rubin Y, AG Jurnel. Simulation of Non-Gaussian Space Random Functions for Modeling
1871 848 Transport in Groundwater. *Water Resources Research*. 27 (1991) 1711-21.
1872 849 [55] Scheibe TD, EM Murphy, X Chen, AK Rice, KC Carroll, BJ Palmer, et al. An analysis platform for
1873 850 multiscale hydrogeologic modeling with emphasis on hybrid multiscale methods. *Ground Water*. 53
1874 851 (2015) 38-56, doi: 10.1111/gwat.12179.
1875 852 [56] Scheibe TD, K Schuchardt, K Agarwal, J Chase, X Yang, BJ Palmer, et al. Hybrid multiscale
1876 853 simulation of a mixing-controlled reaction. *Advances in Water Resources*. 83 (2015) 228-39, doi:
1877 854 10.1016/j.advwatres.2015.06.006.
1878 855 [57] Scheibe TD, X Yang, X Chen, GE Hammond. A Hybrid Multiscale Framework for Subsurface Flow
1879 856 and Transport Simulations. *Procedia Computer Science*. 51 (2015) 1098-107, doi:
1880 857 10.1016/j.procs.2015.05.276.
1881 858 [58] Song H-S, C Liu. Dynamic Metabolic Modeling of Denitrifying Bacterial Growth: The Cybernetic
1882 859 Approach. *Industrial & Engineering Chemistry Research*. 54 (2015) 10221-7, doi:
1883 860 10.1021/acs.iecr.5b01615.
1884 861 [59] Song H-S, D Thomas, M Li, X Song, X Chen, J Stegen, et al. Genetically structured microbial
1885 862 community modeling: Application to denitrification process in hyporheic zone sediments. *Environmental
1886 863 Science and Technology*. in preparation (2017).
1887 864 [60] Song X, J Stegen, GE Hammond, H-S Song, H Dai, E Graham, et al. Dam operation impacts on
1888 865 hyporheic zone reaction rates and thermal environment are maximized under low-flow conditions.
1889 866 *Geophysical Research Letters*. in preparation (2017).
1890 867 [61] Stegen JC, JK Fredrickson, MJ Wilkins, AE Konopka, WC Nelson, EV Arntzen, et al. Groundwater-
1891 868 surface water mixing shifts ecological assembly processes and stimulates organic carbon turnover. *Nat
1892 869 Commun*. 7 (2016) 11237, doi: 10.1038/ncomms11237.
1893 870 [62] Storey RG, KWF Howard, DD Williams. Factors controlling riffle-scale hyporheic exchange flows
1894 871 and their seasonal changes in a gaining stream: A three-dimensional groundwater flow model. *Water
1895 872 Resources Research*. 39 (2003) n/a-n/a, doi: 10.1029/2002wr001367.

1905
1906
1907
1908 [63] Tang Y, AJ Valocchi, CJ Werth. A hybrid pore-scale and continuum-scale model for solute
1909 diffusion, reaction, and biofilm development in porous media. *Water Resources Research*. 51 (2015)
1910 1846-59, doi: 10.1002/2014wr016322.
1911 [64] Thorne PD, MP Bergeron, MD Williams, VL Freedman. Groundwater data package for Hanford
1912 assessments,. Pacific Northwest National Laboratory, Richland, Washington, 2006.
1913 [65] Tomin P, I Lunati. Hybrid Multiscale Finite Volume method for two-phase flow in porous media.
1914 *Journal of Computational Physics*. 250 (2013) 293-307, doi: 10.1016/j.jcp.2013.05.019.
1915 [66] Tomin P, I Lunati. Investigating Darcy-scale assumptions by means of a multiphysics algorithm.
1916 *Advances in Water Resources*. 95 (2016) 80-91, doi: 10.1016/j.advwatres.2015.12.013.
1917 [67] Trauth N, C Schmidt, U Maier, M Vieweg, JH Fleckenstein. Coupled 3-D stream flow and hyporheic
1918 flow model under varying stream and ambient groundwater flow conditions in a pool-riffle system. *Water*
1919 *Resources Research*. 49 (2013) 5834-50, doi: 10.1002/wrcr.20442.
1920 [68] Trauth N, C Schmidt, M Vieweg, U Maier, JH Fleckenstein. Hyporheic transport and
1921 biogeochemical reactions in pool-riffle systems under varying ambient groundwater flow conditions.
1922 *Journal of Geophysical Research: Biogeosciences*. 119 (2014) 910-28, doi: 10.1002/2013JG002586.
1923 [69] Truex MJ, VR Vermeul, BG Fritz, RD Mackley, DP Mendoza, RP Elmore, et al. Hanford 100-D
1924 Area Biostimulation Treatability Test Results. Pacific Northwest National Laboratory, Richland,
1925 Washington, 2009.
1926 [70] USDOE. Hanford Site Groundwater Monitoring and Performance Report for 2009: Volumes 1 & 2.
1927 2010.
1928 [71] van Genuchten MT. A Closed-form Equation for Predicting the Hydraulic Conductivity of
1929 Unsaturated Soils. *Soil Science Society of America Journal*. 44 (1980).
1930 [72] Vermeul VR, MP Bergeron, C Cole, CJ Murray, WE Nichols, TD Scheibe, et al. Transient inverse
1931 calibration of the site-wide groundwater flow model (ACM-2): FY 2003 Progress Report. Pacific
1932 Northwest National Laboratory, Richland, Washington, 2003.
1933 [73] Vermeul VR, BN Bjornstad, BG Fritz, JS Fruchter, RD Mackley, DP Mendoza, et al. 300 Area
1934 Uranium Stabilization Through Polyphosphate Injection: Final Report. Pacific Northwest National
1935 Laboratory, Richland, Washington, 2009.
1936 [74] Wagner BJ, SM Gorelick. Reliable Aquifer Remediation in the Presence of Spatially Variable
1937 Hydraulic Conductivity' From Data to Design. *Water Resources Research*. 25 (1989) 2211-25.
1938 [75] Wilde M, M Hategan, JM Wozniak, B Clifford, DS Katz, I Foster. Swift: A language for distributed
1939 parallel scripting. *Parallel Computing*. 37 (2011) 633-52, doi: 10.1016/j.parco.2011.05.005.
1940 [76] Williams BA, BN Bjornstad, R Schalla, WD Webber. Revised hydrogeology for the suprabasalt
1941 aquifer system, 200-East area and vicinity, Hanford Site, Washington. Pacific Northwest National
1942 Laboratory, Richland, Washington, 2000.
1943 [77] Williams MD, ML Rockhold, PD Thorne, Y Chen. Three-Dimensional Groundwater Models of the
1944 300 Area at the Hanford Site, Washington State. Pacific Northwest National Laboratory, Richland,
1945 Washington, 2008.
1946 [78] Wood BD. The role of scaling laws in upscaling. *Advances in Water Resources*. 32 (2009) 723-36,
1947 doi: 10.1016/j.advwatres.2008.08.015.
1948 [79] Yan S, Y Liu, C Liu, L Shi, J Shang, H Shan, et al. Nitrate bioreduction in redox-variable low
1949 permeability sediments. *Sci Total Environ*. 539 (2016) 185-95, doi: 10.1016/j.scitotenv.2015.08.122.
1950
1951
1952
1953
1954
1955
1956
1957
1958
1959
1960

1961
1962
1963 915 [80] Yang X, Y Mehmani, WA Perkins, A Pasquali, M Schönherr, K Kim, et al. Intercomparison of 3D
1964 916 pore-scale flow and solute transport simulation methods. *Advances in Water Resources*. 95 (2016) 176-
1965 917 89, doi: 10.1016/j.advwatres.2015.09.015.
1966 918 [81] Young JD, D Ramkrishna. On the matching and proportional laws of cybernetic models. *Biotechnol
1967 Prog.* 23 (2007) 83-99, doi: 10.1021/bp060176q.
1969 920 [82] Zachara JM, MD Freshley, GV Last, RE Peterson, BN Bjornstad. Updated Conceptual Model for the
1970 921 300 Area Uranium Groundwater Plume. Pacific Northwest National Laboratory, Richland, Washington,
1971 922 2012.
1972 923 [83] Zachara JM, PE Long, J Bargar, JA Davis, P Fox, JK Fredrickson, et al. Persistence of uranium
1973 924 groundwater plumes: contrasting mechanisms at two DOE sites in the groundwater-river interaction zone.
1974 925 *J Contam Hydrol.* 147 (2013) 45-72, doi: 10.1016/j.jconhyd.2013.02.001.
1976
1977
1978
1979
1980
1981
1982
1983
1984
1985
1986
1987
1988
1989
1990
1991
1992
1993
1994
1995
1996
1997
1998
1999
2000
2001
2002
2003
2004
2005
2006
2007
2008
2009
2010
2011
2012
2013
2014
2015
2016